

Review

Research Progress on the Influence of Cathode Materials on Thermal Runaway Behavior of Lithium-Ion Batteries

Yanru Yang ^{1,2}, Yang Gao ^{2,3,*}, Yu Miao ^{1,2}, Yuan Liang ^{2,3} and Xiaoqiang Ren ^{2,3}

¹ School of Electrical and Information Engineering, North Minzu University, Yinchuan 750021, China; 20247397@stu.nmu.edu.cn (Y.Y.); 20237383@stu.nmu.edu.cn (Y.M.)

² Ningxia Engineering Research Center for Hybrid Manufacturing System, Yinchuan 750021, China; 2021726@nmu.edu.cn (Y.L.); 2024524@nmu.edu.cn (X.R.)

³ College of Mechatronic Engineering, North Minzu University, Yinchuan 750021, China

* Correspondence: 2008034@nmu.edu.cn; Tel.: +86-18009595561

Abstract

The structure, chemical composition, thermal stability, and abuse responses of cathode materials are critical to the safety and economy of lithium-ion batteries (LIBs). This review systematically summarizes advances in research on how cathode materials influence LIB thermal runaway (TR) behavior. It analyzes the oxygen release from cathodes in TR mechanisms and the hazards of such oxygen generation during TR, expounds on how differences in cathode structure, chemical composition, and thermal stability affect TR behavior, and summarizes the thermal characteristics of LIBs with different cathodes under mechanical, electrical, and thermal abuse. Results indicate that oxygen released from cathode decomposition during TR oxidizes electrolytes, releasing substantial heat and gas and causing more severe TR hazards. Structural instability of cathodes leads to accelerated release of lattice oxygen, speeding up TR initiation. Chemical composition regulates thermal stability, phase transition pathways, and gas generation rates during TR, while elemental ratios affect the ease of TR triggering. Cathodes with poor thermal stability have lower thermal decomposition onset temperatures, making TR more likely to occur and intensifying reaction severity. All three abuse types trigger inherent risks of cathodes, inducing TR and significantly increasing its occurrence probability. Differences in intrinsic properties further extend to the system level, also influencing thermal runaway propagation and fire dynamics at the module level. Future research focusing on the intrinsic properties of cathodes and external abuse is of great significance for addressing LIB TR behavior.



Academic Editor: Hirotoshi Yamada

Received: 8 September 2025

Revised: 5 October 2025

Accepted: 10 October 2025

Published: 12 October 2025

Citation: Yang, Y.; Gao, Y.; Miao, Y.; Liang, Y.; Ren, X. Research Progress on the Influence of Cathode Materials on Thermal Runaway Behavior of Lithium-Ion Batteries. *Batteries* **2025**, *11*, 373. <https://doi.org/10.3390/batteries11100373>

Copyright: © 2025 by the authors. Licensee MDPI, Basel, Switzerland. This article is an open access article distributed under the terms and conditions of the Creative Commons Attribution (CC BY) license (<https://creativecommons.org/licenses/by/4.0/>).

Keywords: lithium-ion battery; thermal runaway; cathode material; intrinsic properties; abuse behavior; thermal runaway propagation; safety

1. Introduction

With the increasing demand for electronic products and the widespread use of electric vehicles, lithium-ion batteries (LIBs) have become increasingly common as one of the most promising power sources [1,2]. The development of lithium-ion batteries with diverse cathode materials [3] to meet safety application requirements in different scenarios and address resource and environmental issues is a primary goal for current researchers. However, different commercial Li-ion battery cathode materials have different chemical compositions, properties, costs, and thermal characteristics [4]. When lithium-ion batteries (LIBs) are exposed to non-standard operating regimes, this predisposes them to thermal

runaway (TR) events, thereby compromising societal safety and infrastructural integrity. Consequently, a comprehensive investigation into the TR characteristics across distinct cathode chemistries constitutes a critical research priority for advancing battery safety protocols and state-of-health management frameworks.

Researchers widely recognize four key mechanisms as critical drivers of TR in LIBs: decomposition of the solid-electrolyte interphase (SEI), oxidative breakdown at the anode–electrolyte interface, cathode–electrolyte reactions [5], and bulk electrolyte degradation [6–10]. The cathode material critically governs TR progression in LIBs. Maleki et al. [11] demonstrated through accelerating rate calorimetry (ARC) of laboratory-scale full cells that exothermic interactions between cathode active materials and electrolytes serve as the primary trigger for TR initiation. Liu et al. [12] examined the TR mechanism in automotive batteries at both the battery cell level and material scale, revealing the crucial role of chemical crosstalk between positive and negative electrodes. Jhu et al. [13] stated that the overall thermal response of the battery is dictated by the cathode material, revealing that this component primarily governs the magnitude of heat generation.

As the largest oxidizer and energy carrier in the battery system, the TR behavior of anode materials directly dominates the triggering and propagation path of TR. A comprehensive investigation into the regulation mechanism of TR in cathode materials is crucial for overcoming the safety limitations of batteries. Cathode materials of LIBs are primarily made up of lithium transition metal oxides. These include lithium iron phosphate (LiFePO_4), lithium manganate (LiMn_2O_4), lithium cobaltate (LiCoO_2), as well as cobalt-containing multi-component oxides like lithium-nickel-manganese-cobalt oxide (NMC) and lithium-nickel-cobalt-aluminum oxide (NCA) [14]. In research on the TR mechanism, it has been observed that the liberation of lattice oxygen from cathode materials under high-temperature conditions serves as the core trigger for thermal runaway. Moreover, the oxygen liberation process, accompanied by heat release, constitutes the key factor leading to combustion and explosion during battery TR. For example, the NMC811 cathode boasts notable advantages in high energy capacity; however, its early oxygen release behavior is regarded as a major safety risk in the use of high-nickel layered cathode materials [15]. An in-depth explanation of the correlation between the oxygen behavior and the intrinsic properties of materials represents a breakthrough in reducing the incidence of TR. The inherent characteristics of cathode materials act as the core factors that determine TR performance; meanwhile, the structural type exerts an influence on the thermal stability of cathode materials to a certain degree. Again, it should be noted that olivine, spinel, and layered structures are typical cathode material structures. Lithium-ion batteries made of layered metal oxides are highly susceptible to low-temperature oxygen release and have the greatest risk of thermal runaway [16]. For cathode materials sharing the same layered structure, variations in their phase transition pathways significantly influence both the timing of TR initiation and the extent of oxygen evolution. The chemical composition (types and ratios of elements) precisely modulates the thermal runaway characteristics of cathode materials. Elevating Ni concentration in layered NCM cathodes detrimentally impacts electrochemical and thermal durability [17]; consequently, optimizing LIB performance necessitates a more critical focus on achieving stoichiometric balance among constituent elements. Cathode material thermal tolerance governs their thermal runaway behavior, with characteristic parameters serving as quantifiable TR risk indicators alongside inherent composition and structural properties. Consequently, identifying cathode materials exhibiting optimal thermal stability alongside targeted electrochemical properties constitutes a critical research objective [18].

The inherent risk of cathode materials can be triggered by external abuse. TR can initiate under extreme scenarios where a battery's internal heat generation rate surpasses

its ambient heat dissipation capacity, and these critical conditions encompass mechanical, electrical, and thermal abuse modes [6,8,19–25]. Mechanical abuse scenarios principally involve perforation, compression, and flexural deformation, inducing separator rupture and consequent internal short circuits [26], testing the response of anode materials to localized high temperatures. Electrical abuse mainly consists of overcharging and overdischarging, which usually makes Li-ion batteries less thermally stable or short-circuited [26]. When the battery is overheated, it leads to thermal abuse, which triggers a series of exothermic reactions when it reaches a certain temperature [26], with the pivotal factor residing in the critical transition point of the material's inherent thermal stability. As shown in Figure 1. It is worth noting that not all lithium-ion batteries with different cathode materials combust upon thermal runaway; compared to layered oxide batteries, LFP batteries exhibit a milder response, typically releasing only white smoke.

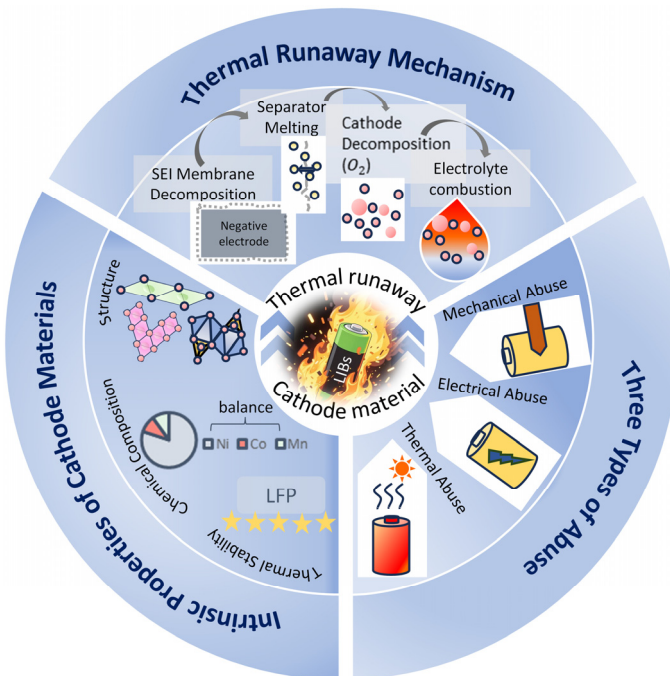


Figure 1. Thermal runaway mechanism properties of cathode materials, intrinsic properties of cathode materials, and three kinds of abuse triggering thermal runaway.

The intrinsic properties of cathode materials not only influence the severity of thermal runaway at the individual cell level but also extend to the system level, affecting the propagation of thermal runaway and the nature of fires. Layered cathode materials, with their intense oxygen release behavior, often generate large amounts of combustible gases and jet flames, accelerating thermal runaway propagation within the module. In contrast, cathodes with stable framework structures, such as LFP, exhibit entirely different behavior. Therefore, understanding the comprehensive impact of cathode materials from the cell to the module and even the system scale is particularly important in the study of battery safety systems.

Conventional research often treats the cathode as a single component within the broader lithium-ion battery system. In contrast, this study establishes a thermal runaway analysis framework that places cathode materials at its core. Given their pivotal role, cathode materials are examined in isolation, disentangled from the intricate interplay with the anode and electrolyte. Key properties—including crystal structure stability, chemical composition, and the release of reactive oxygen species during phase transitions—directly govern the onset temperature, severity, and hazard characteristics of thermal runaway. By

focusing on the cathode material itself, this review organizes the mechanistic features of thermal runaway in lithium-ion battery cathodes. It elucidates the influence of the material's internal structure, chemical composition, and thermal stability on thermal runaway behavior. Furthermore, it analyzes the manifestations of thermal runaway when intrinsic material risks are activated under external abuse conditions, as well as the differences in combustion and ignition behavior among various cathode materials due to their distinct intrinsic properties. The discussion is elevated from the cell level to the broader implications at the module and system levels. It summarizes the challenges in optimizing cathode materials to address the thermal runaway issue in lithium-ion batteries and discusses future research prospects and potential breakthroughs.

2. Thermal Runaway Mechanism Characteristics of Cathode Materials

2.1. Triggering and Evolution Mechanism of Thermal Runaway

Battery thermal runaway may occur under puncture, crush, overcharge, overdischarge, and overheating, and in extreme environments, the battery undergoes diaphragm failure, which leads to an internal short circuit (ISC) [6]. An ISC initiates runaway heating within the cell, triggering a cascade of exothermic reactions. This rapid energy discharge leads to intense temperature spikes. When heat accumulation exceeds dissipation, the situation can culminate in thermal runaway (TR) [27–29]. Figure 2a illustrates the thermal runaway initiation process in lithium-ion batteries under three abuse conditions.

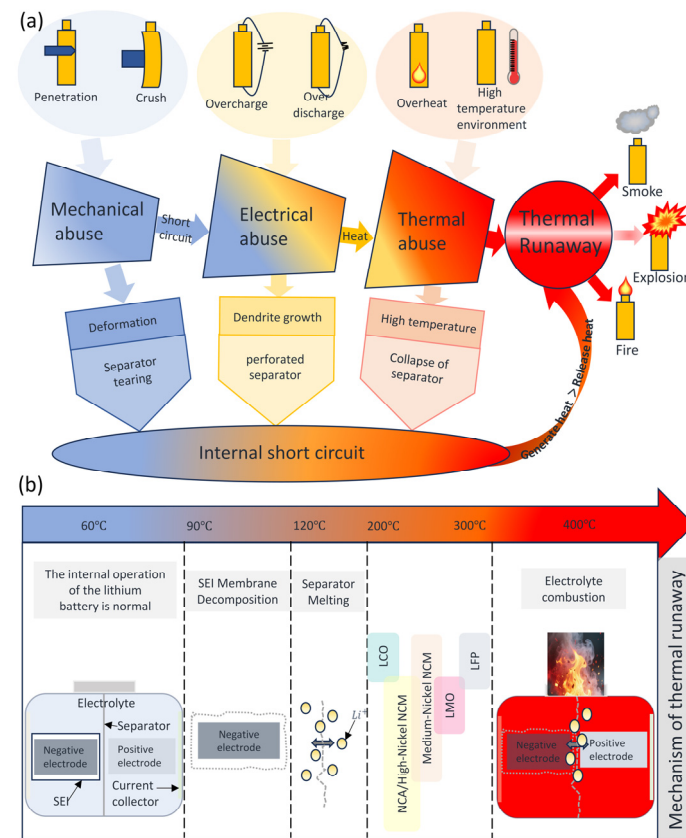


Figure 2. (a) The Process of Triggering Thermal Runaway; (b) Mechanism of thermal runaway.

Thermal runaway is a failure mechanism [6]. Initiating thermal runaway, the metastable solid electrolyte interphase (SEI) undergoes exothermic decomposition around 60–90 °C, releasing gases including carbon dioxide (CO₂), oxygen (O₂), and ethylene (C₂H₄) [30]. Above 90 °C, SEI decomposition initiates [31] and serves as a primary driver of thermal runaway in batteries [32]. Its decomposition not only liberates heat, elevating

the battery temperature [33], but also strips the negative electrode active material of its protective layer. This exposure allows sustained exothermic side reactions upon direct electrolyte exposure [34]. Above 120 °C, the separator collapses via thermal shrinkage, and melting induces massive internal short circuits, compromising lithium-ion isolation from the anode and triggering violent electrolyte reactions that generate localized hotspots through intense exothermic processes [12,35]. In most cases, thermal runaway (TR) events are triggered by ISCs [5]. As the temperature rises, the electrolyte undergoes continuous decomposition. Cathode materials with poor thermal stability decompose slightly upon heating, releasing oxygen. The electrolyte subsequently undergoes exothermic reactions with cathodically liberated O₂, accelerating temperature escalation through heat release. Cathode materials with good thermal stability start to decompose at higher temperatures. As the degree of lithium deintercalation from the cathode deepens, thermal decomposition intensifies, causing the cathode material to release more oxygen. Acting as a potent oxidant, O₂ drives vigorous oxidation of electrolytic solvents, liberating substantial exothermic energy and gaseous products. Simultaneous electrolyte reactions with cathode/anode active materials initiate at this stage, driving exponential heating rate acceleration that culminates in potential explosion and thermal runaway [13,16,36,37]. The staged exothermic reactions exhibit non-sequential characteristics, potentially occurring concurrently with significant synergistic coupling [16]. The progression of thermal runaway is schematically represented in Figure 2b.

2.2. Role of Cathode Materials in Thermal Runaway

2.2.1. Hazards of Cathode Materials

The positive electrode is the most dangerous component during thermal runaway occurrence [38]. High-temperature cathode degradation constitutes a primary accelerator in thermal runaway cascades, with liberated oxygen functioning as reactive flux. Mao et al. [38] demonstrated that heat generation from the cathode constitutes the dominant contribution to total battery heat release. Liu et al. [12] employed differential scanning calorimetry (DSC) to quantify the rapid thermal response upon oxygen exposure. Their measurements confirmed that significant heat release from the cathode originates from oxygen liberation during material decomposition. Furthermore, cathode decomposition fundamentally involves structural destabilization in highly delithiated states under thermal stress. This delithiated-state thermal stability directly governs battery safety [39]. Enhancing cathode structural integrity suppresses oxygen evolution and reduces total heat generation [40].

2.2.2. Sources and Hazards of Oxygen

Metal oxide cathodes evolve oxygen under thermal stress [41]. Li et al. [42] identified cathode-originating oxygen species (O₂²⁻, O₂⁻, O⁻) as the primary driver of TR, demonstrated in NCM811-cathode lithium-ion batteries. Lattice oxygen (O²⁻) in cathode materials remains structurally stabilized within transition metal (Ni, Co, Mn) crystal frameworks under normal conditions. Elevated temperatures energize lattice oxygen, forming charged states (O⁻, O₂⁻) that remain confined within lattice sites as chemisorbed species. Further heating enables oxygen migration from the lattice, generating surface-bound O₂ through physisorption. This triggers subsequent oxygen liberation from particle surfaces.

The release of oxygen is a serious and long-standing problem [43–45] that can trigger dangerous combustion reactions [46]. Liu et al. [12] considered oxygen as the most dangerous gas. Internal oxygen sources from cathodes critically constrain fire suppression upon thermal runaway initiation [12]. Liu et al. [47] established that cathodes in deeply delithiated states experience pronounced oxygen release. The liberated oxygen then chemi-

cally interacts with electrolyte and anode constituents, resulting in substantial heat release during these interactions. Zhang et al. [48] employed accelerating rate calorimetry (ARC) to analyze thermal runaway behavior in fully charged NCM811 batteries under elevated temperatures. Their findings revealed that peak temperatures and maximum heating rates during runaway events are primarily governed by reactions between cathode-derived oxygen and the electrolyte. All lithium-ion battery cathode materials demonstrate thermal degradation susceptibility under elevated temperatures, where liberated oxygen initiates autocatalytic electrolyte reactions [13]. This contributes to the fire or explosion of flammable alkyl carbonate solvents in the electrolyte [46]. Liu et al. [12] identified cathode-originated oxygen as a reactive agent with anode substances, generating critical safety risks. During thermal runaway acceleration, oxygen consumption by electrolyte and anode components produces massive gaseous products. This gas accumulation represents the dominant explosion initiator [4]. Figure 3a–c depict dynamic conversion processes of oxygen species at charged cathodes across different materials. Panels illustrate: (a) oxygen evolution pathways without electrolyte, and (b,c) oxidative interactions between reactive oxygen species and abundant electrolyte under high-reactivity conditions.

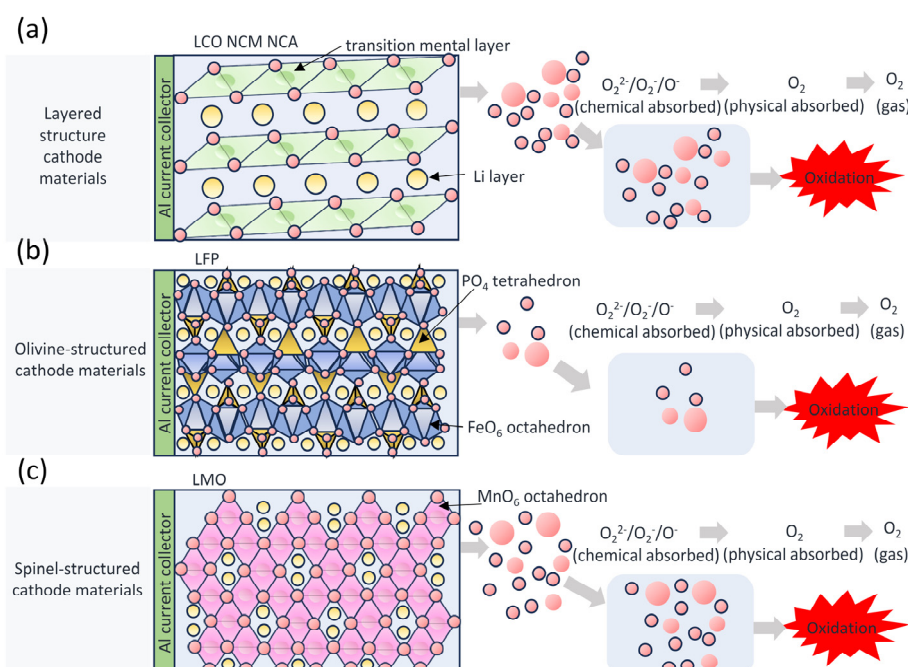
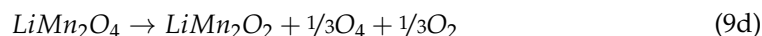
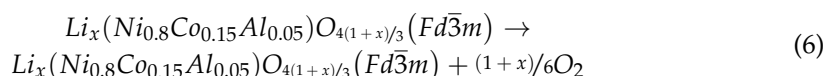
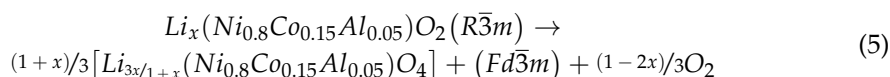
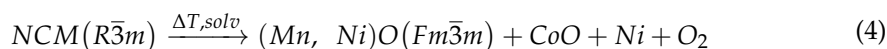
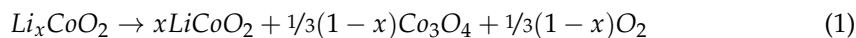


Figure 3. Oxygen Formation Process of Cathode Materials: (a) LCO, NCM, NCA; (b) LFP; (c) LMO in the Absence of Electrolyte, and Oxidation Process of Electrolyte by Oxygen Species in the Presence of Electrolyte.

2.2.3. Differences in Oxygen Release of Cathode Materials

The quantity of oxygen released by cathode materials constitutes a pivotal step in the TR mechanism of LIBs. Cathode materials with a higher oxygen release amount are likely to generate more heat, causing greater harm. Liu et al. [12] used the heat production curve measured by differential scanning calorimetry (DSC) and the variation of oxygen release with temperature characterized by mass spectrometry (MS) as in Figure 4. Oxygen evolution from cathode materials coincides with exothermic processes, exhibiting significant correlation within specific temperature ranges. For different cathode materials, the amount and rate of oxygen release show differences. Belharouak et al. [49] investigated oxygen evolution behavior in chemically delithiated ternary cathodes: $Li_{0.45}(Ni_{0.8}Co_{0.15}Al_{0.05})O_2$ (NCA-0.45) and $Li_{0.55}(Ni_{1/3}Co_{1/3}Mn_{1/3})O_2$ (NCM-0.55). Analysis revealed slower oxygen release kinetics in NCM-0.55 during thermal treatment, whereas NCA-0.45 exhibited

accelerated oxygen liberation. Monteiro et al. [50] concluded that no oxygen is released when LFP decomposes at high temperatures. However, Ping, Wang et al. [51,52] proposed that, when LiFePO₄ is heat-treated at temperatures up to 350 °C, it decomposes from its delithiated state into Fe₂P₂O₇ and releases oxygen. Furthermore, Lamb et al. [19] conducted calorimetric analysis on charged LFP cathodes, and the results showed that LFP releases less oxygen per delithiated site and has a lower heat release compared to layered metal oxides. Huang, Faulkner et al. [7,53] investigated comparative oxygen evolution from prevalent cathode systems (LCO, NMC, NCA, LFP), revealing NCA materials exhibit the highest oxygen liberation capacity. Lamb et al. [19] quantified oxygen liberation from delithiated sites across varied cathode systems. Their analysis established that sufficiently heated layered metal oxides transform into rock salt structures, releasing one oxygen atom per delithiation site. For lithium iron phosphate (LFP), quantification studies indicate 0.5 oxygen atoms liberated per site during decomposition. Lithium manganate (LMO) exhibits variable oxygen release, with proposed values of 2 or 1 atom per delithiation site. Divergent findings exist regarding oxygen yield per delithiation site in lithium manganate (LMO) decomposition, with proposals of either two or one oxygen atom release. Chemical Equations (1–9) describing thermal decomposition pathways for common cathode materials are provided [54], where LiMn₂O₄ decomposition follows reaction Schemes (8) or (9a–d). To mitigate the hazards associated with oxygen, embedded oxygen sensors can be developed for real-time thermal runaway warning by monitoring changes in ambient oxygen concentration. Furthermore, future efforts should focus on designing cathode materials with low or no oxygen release to suppress reactions between oxygen and the electrolyte. Optimizing the electrolyte formulation, such as incorporating flame retardants, can help curb combustion initiated by oxygen release. Alternatively, replacing organic liquid electrolytes with chemically more stable solid electrolytes could eliminate the risk of violent reactions between oxygen and the electrolyte.



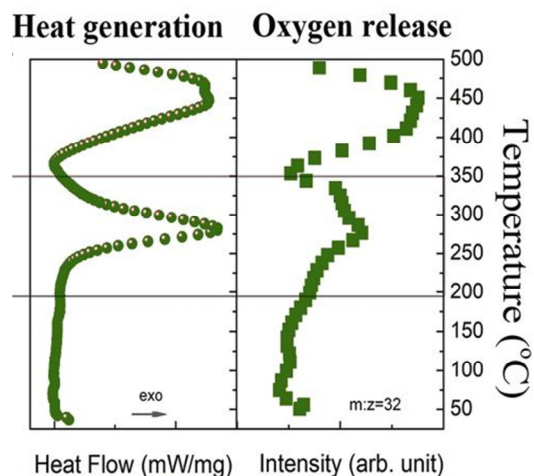


Figure 4. Curves of heat generation and oxygen release from the charged cathode as a function of temperature [12].

3. Influence of Intrinsic Properties on Thermal Runaway Behavior of Lithium-Ion Batteries

3.1. Influence of Structure on Thermal Runaway Behavior

The structural configuration of cathode materials plays a critical role in determining the safety performance of lithium-ion batteries (LIBs) [50]. Specifically, the crystal structure type governs the intrinsic thermal stability of these materials, thereby influencing both the onset temperature and the severity of thermal runaway events in LIBs. Different structures of cathode materials have different binding capacity of lattice oxygen and different paths of structural evolution at high temperatures, making the oxygen release behavior and thermal runaway risk different.

3.1.1. Structural Type Determines Thermal Stability

The crystal structure framework of cathode materials determines their ability to bind oxygen atoms and structural stability, which forms the basis for the thermal stability of cathode materials. Common structures include layered oxides, olivine structures, and spinel structures [10]. Among cathode materials for lithium-ion batteries, layered structures (hexagonal NaFeO₂-type, space group $R\bar{3}m$) are adopted by LiCoO₂ (LCO), LiNi_{1-x-y}Mn_xCo_yO₂ (NMC), and LiNi_{1-x-y}Al_xCo_yO₂ (NCA). In contrast, LiFePO₄ (LFP) is structured in the olivine type (orthorhombic, space group Pnma), while LiMn₂O₄ (LMO) is characterized by a spinel framework (cubic, space group $Fd\bar{3}m$). Due to their structural characteristics, layered oxides exhibit the poorest thermal stability, olivine structures demonstrate excellent thermal stability [2,10,55–58], and spinel structures fall in between [2,10,55–58], and spinel structures fall in between.

Layered structures are a major source of high risk of thermal runaway due to their relatively weak interlayer forces and susceptibility to delithiation [16]. Exhibiting limited thermal stability, these cathode materials typically initiate decomposition during thermal runaway, with the onset typically occurring between approximately 180 °C and 200 °C. They release oxygen prematurely to react with the electrolyte, accompanied by a sharply accelerated exothermic reaction rate, which ultimately leads to high-rate thermal runaway events [19,59]. Compared with layered cathode materials, LiFePO₄ (LFP) with an olivine structure releases less oxygen and heat. Zaghib et al. [59] proposed that, under thermal runaway conditions, LFP initially transforms into iron phosphate (FePO₄). The heat generated by the combustion of electrolyte solvent and released oxygen serves to stabilize the FePO₄ phase, which in turn sustains the structural integrity of the LiFePO₄/FePO₄

cathode system. The olivine structure features a stable PO_4 tetrahedral framework. In LiFePO_4 , the $(\text{PO}_4)^{3-}$ polyanions underpin the structural integrity of the olivine framework. Furthermore, the strong covalent bonding within the P-O units exhibits high resistance to thermal degradation, effectively suppressing oxygen loss and consequently leading to a significantly reduced rate of oxygen release. The cathode material releases the least amount of oxygen during decomposition, which not only weakens its own combustion process but also avoids further damage to the cathode structure [30,58,60]. Yu et al. [57] investigated the structural evolution of three cathode materials—specifically layered L523 (referred to as NCM523 herein), olivine-structured LFP, and spinel-structured LMO—subjected to three distinct conditions: room temperature (RT), 350 °C, and 350 °C with electrolyte present. The corresponding X-ray diffraction (XRD) spectra for these cathodes under the varying thermal and chemical environments are presented in Figure 5. Upon heating the pristine cathode samples to 350 °C, the olivine framework of LiFePO_4 (LFP) was observed to retain its original configuration; LMO maintained its basic structure except for the formation of a small amount of Mn_3O_4 , while L523 showed the appearance of a spinel phase. Within the combined thermal and electrolyte environment at 350 °C, the incorporation of lithium salts into the organic solvent (forming the electrolyte) was found to enhance the decomposition kinetics of both LMO and LFP while suppressing the degradation of L523 (NCM523). Under this environment, all three materials exhibited phenomena such as broadening, weakening, or even disappearance of the original diffraction peaks, but the structure of LFP remained highly stable.

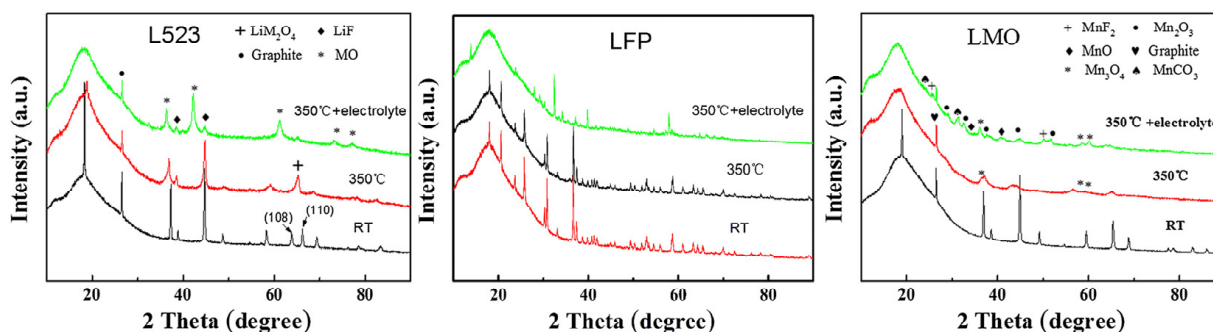


Figure 5. XRD patterns of L523, LFP, and LMO at room temperature, 350 °C, and 350 °C + electrolyte environment, respectively [57].

3.1.2. Mechanisms of Destabilization of Layered Structures

The inferior thermal robustness observed in layered transition metal oxides originates primarily from their inherent structural instability under elevated temperatures and during the delithiated state. Progressive delithiation induces structural destabilization, phase transitions, and cation migration/mixing within the lattice. This progressive loss of lithium ultimately culminates in the release of oxygen from the crystal lattice, as the structure becomes increasingly unstable. For Li_xCoO_2 , it undergoes a multistage phase transition as x decreases (lithium-ion detachment). When $x > 0.75$, LCO transforms from one O_3 phase to another. Upon further reduction of lithium content approaching $x = 0.5$, LiCoO_2 (LCO) experiences a structural reorganization. This involves a conversion from the initial hexagonal arrangement (designated O_3) to a monoclinic structure (designated M). During this transformation, the oxygen sublattice rearranges from hexagonal close-packing (HCP) to face-centered cubic (FCC) stacking, concomitant with cation migration within the lattice [61,62]. Alterations in the oxygen stacking configuration enhance the reactivity of oxygen species, contributing to the release of oxygen from the lattice [62]. Furthermore, the rearrangement of cations (specifically Li^+ and Co^{4+}) to establish a monoclinic structure

is considered a primary contributor to the structural instability observed in LCO. The low symmetry of the monoclinic phase increases the lattice stress, making the material more susceptible to thermally stimulated decomposition, release of oxygen, and violent reaction with the electrolyte, etc., and triggering subsequent exothermic reactions. At lithium contents below $X < 0.45$, the material transitions from the O3 structure (where the M phase represents a distorted intermediate state occurring at moderate delithiation) to the H1-3 phase. Further reduction of lithium content ultimately results in the formation of a mixed-phase configuration comprising both H1-3 and O1 phases. The crystal structure phase transition pattern of LCO with decreasing lithium ion content during the delithiation process is shown in Figure 6 [63]. The combined effects of phase transformations and cationic disordering/rearrangement during the degradation of the layered framework compromise the lattice-oxygen bonding. This structural collapse occurs concurrently with oxygen evolution, a process that serves as a key contributing factor to the initiation of thermal runaway.

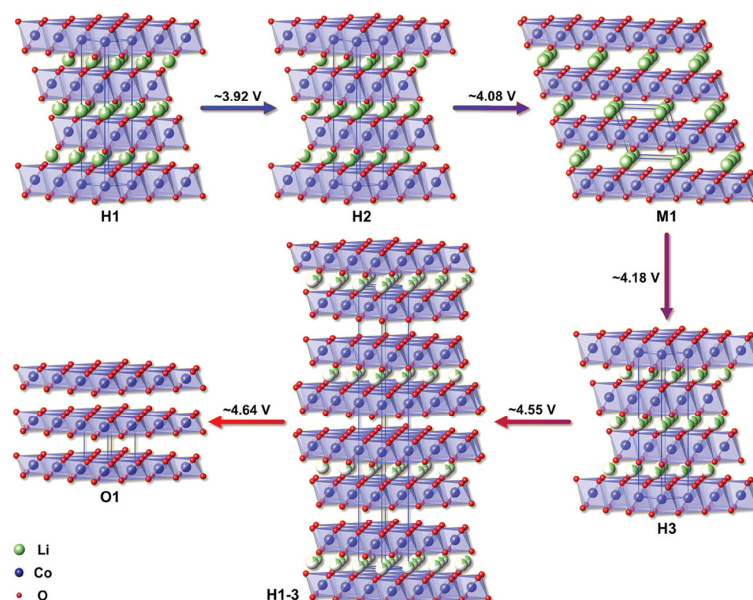


Figure 6. Crystal structure phase transition law during the LCO delithiation process [63].

3.1.3. Influence of Phase Transition Path Differences on Thermal Runaway Behavior

The specific high-temperature phase evolution pathways exhibited by different layered cathode materials profoundly influence their thermal runaway propensity. Among the phase transformation routes identified for layered Ni-Co-Mn (NCM) and Ni-Co-Al (NCA) oxide cathodes, those associated with NCA present significantly elevated safety concerns, in stark contrast to the superior thermal stability demonstrated by NCM. Belharouak et al. [49] investigated the oxygen release behavior of ternary cathode materials after chemical delithiation by thermogravimetric analysis (TGA), using XRD to detail the structural evolution from room temperature to 900 °C. Studies revealed that the $\text{Li}_{0.45}(\text{Ni}_{0.8}\text{Co}_{0.15}\text{Al}_{0.05})\text{O}_2$ (NCA) cathode undergoes a rapid phase evolution. This process is characterized by the emergence of spinel characteristics and structural disorder at 265 °C (accompanied by 2 wt% oxygen loss), development of a well-defined spinel structure at 360 °C (4 wt% oxygen loss), transition to a disordered $\alpha\text{-NaFeO}_2$ configuration at 450 °C (9.2 wt% oxygen loss), and ultimately conversion to a rock-salt structure at 900 °C (total oxygen release reaching 11 wt%). This accelerated structural disordering and premature oxygen release in NCA are primarily attributed to cation mixing and lithium migration [50]. In contrast, the $\text{Li}_{0.55}(\text{Ni}_{1/3}\text{Co}_{1/3}\text{Mn}_{1/3})\text{O}_2$ (NCM) cathode maintained its structural integrity up to 175 °C.

The disordered α -NaFeO₂ configuration only emerged at 360 °C (accompanied by 2.5 wt% oxygen loss), while the spinel phase (with 5.8 wt% oxygen loss) was detected at the higher temperature of 540 °C. This NCM material exhibited a more gradual structural disordering process and a delayed onset temperature for thermal runaway, contributing to its superior thermal stability. Nam et al. [61] studied the delithiated nickel-cobalt-aluminum (Ni-Co-Al, NCA) and the results showed that its phase transformation process is from layered phase to a mixed phase of spinel and rock salt, culminating in the formation of a rock-salt phase at elevated temperatures, as depicted in Figure 7a. Moreover, the transformation temperatures are relatively low, with the spinel phase starting at approximately 212 °C and the rock salt phase starting at around 256 °C. Li_{0.33}NCA exhibits a continuous and significant low-energy displacement above 250 °C, and its structural evolution usually tends to transition to the rock salt phase faster and more directly, resulting in a high heat generation rate in the pre-thermal runaway stage. For the NCM811 cathode material, two distinct exothermic peaks are observed. These peaks correspond to the sequential structural reorganization of the cathode, evolving from a layered configuration, through a spinel intermediate phase, and finally to the rock-salt structure [58,64,65]. Nam et al. [61] further explored the phase transformation sequence in electrochemically delithiated nickel-cobalt-manganese (NCM) oxide cathodes, as visualized in Figure 7b. Their findings demonstrated a sequential evolution: initial conversion to a LiM₂O₄-type spinel configuration (onset ~216 °C), followed by progression to a Co₃O₄-type spinel structure (>400 °C), with incomplete structural conversion to the rock-salt phase still evident at 600 °C. Crucially, the Co₃O₄-type spinel intermediate is proposed as the key contributor to NCM's enhanced thermal stability. This phase acts as a critical buffer, significantly delaying progression toward the rock-salt structure. Furthermore, the emergence of the Co₃O₄-type spinel phase correlates with a reduced heat generation rate and extends the pre-thermal-runaway warning period. The NCA cathode lacks this stabilizing intermediate phase, undergoing accelerated degradation directly into the rock-salt structure. Structural progression in cathode materials during thermal runaway involves multiple coupled processes, with NCM and NCA exhibiting distinct phase evolution pathways despite sharing the layered framework common to ternary cathode systems. The phase transition paths can further finely regulate the intensity of thermal runaway, and understanding the correlation between the specific phase transition paths and thermal runaway behaviors of different cathode materials is crucial for the design of cathode materials with higher intrinsic safety.

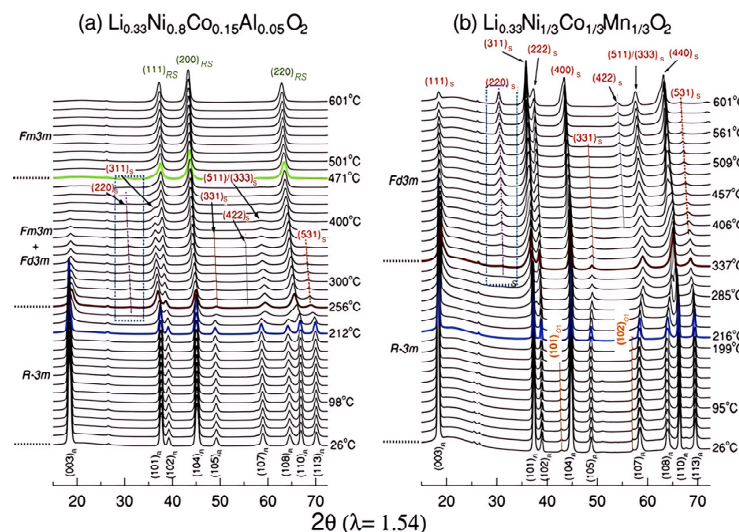


Figure 7. XRD patterns of (a) NCA and (b) NCM cathode materials in delithiated state heated to 600 °C [61].

3.2. Effect of Chemical Composition on Thermal Runaway Behavior

The chemical composition of cathode materials profoundly impacts lithium-ion battery TR behavior [19,66]. Specifically, the ratios of constituent elements—particularly transition metals including Ni, Co, and Mn—directly govern critical properties such as thermal stability and oxygen evolution behavior. These characteristics consequently govern battery TR progression. Layered ternary cathode systems comprise lithium transition metal oxides, predominantly categorized as nickel-cobalt-aluminum (NCA) and nickel-cobalt-manganese (NCM) formulations [67]. Among the chemical elements in the cathode materials of NCM ternary batteries, the content of nickel (Ni) largely determines the capacity, cathode performance, and thermal stability of the ternary batteries [3,68]. NCM cathodes represent the most prevalent ternary system designed to optimize performance trade-offs through compositional tuning of nickel (Ni), cobalt (Co), and manganese (Mn) constituents. The Ni/Mn/Co stoichiometry [69] critically governs thermal runaway propensity through its modulation of cathode decomposition kinetics, oxygen evolution characteristics, and crystalline stability.

3.2.1. Bifacial Characterization of High-Nickel Cathode Materials

Among the chemical element compositions of NCM ternary cathode materials, nickel content has the most significant effect on thermal stability. While increased nickel content elevates specific capacity, high-nickel cathodes exhibit compromised thermal stability characterized by reduced decomposition temperatures, intensified heat generation, accelerated oxygen evolution, and diminished thermal stability. This degradation profile directly elevates thermal runaway susceptibility in such materials. Zhang et al. [70] concluded that the thermal decomposition temperature of NCM materials with increasing nickel content will gradually decrease, while the exothermic amount will gradually increase. Hu et al. [55] established that elevated nickel content in cathodes correlates with destabilization of tetravalent nickel species, which triggers premature oxygen evolution, inducing both decreased oxygen loss onset temperatures and significantly amplified oxygen release intensity [42]. Wang et al. [71] performed thermal runaway testing on NCM111, NCM523, and NCM622 cathodes using EV-ARC. Their analysis revealed increased total heat release with rising nickel content during thermal events. As evidenced in Figure 8, higher nickel loading corresponds to: reduced self-heating onset temperature; diminished material thermal stability; elevated peak thermal runaway temperature. The intrinsic mechanism involves enhanced lithium extraction from high-nickel NCM cathodes versus low-nickel counterparts at equivalent operating voltages during battery operation. This promotes accumulation of the strong oxidant Ni^{4+} , which triggers electrolyte oxidation with concomitant oxygen generation, ultimately diminishing structural stability [70]. Furthermore, nickel exhibits the highest instability among transition metals during thermal decomposition, undergoing the most extensive and rapid reduction from Ni^{4+} to Ni^{2+} [72]. This abrupt valence change disrupts the charge equilibrium in the transition metal layer, inducing release of lattice oxygen as O_2 or O^- species. In addition, the comparable ionic radii of Ni^{2+} (0.076 nm) and Li^+ ions promote lithium-nickel cation mixing [70]. Zhao et al. [73] demonstrated that elevated nickel content (e.g., in NCM811, NCM955 cathodes) promotes internal thermal runaway through reduced anode thermal stability. This effect was quantified by analyzing inter-component energy release and external combustion of evolved combustible gases. Conversely, low-nickel systems exhibit heightened susceptibility to electrolyte reduction reactions, generating increased combustible gas volumes that elevate explosion hazards. Sun et al. [66] reported that the precise interplay between thermal stability in high-nickel cathodes and lithium-ion battery thermal runaway behavior remains incompletely elucidated. However, most researchers believe that high-nickel

cathodes consistently exhibit poorer thermal stability compared to their low-nickel analogs, regardless of control over cutoff voltage or degree of delithiation [30,45,55,68,74,75].

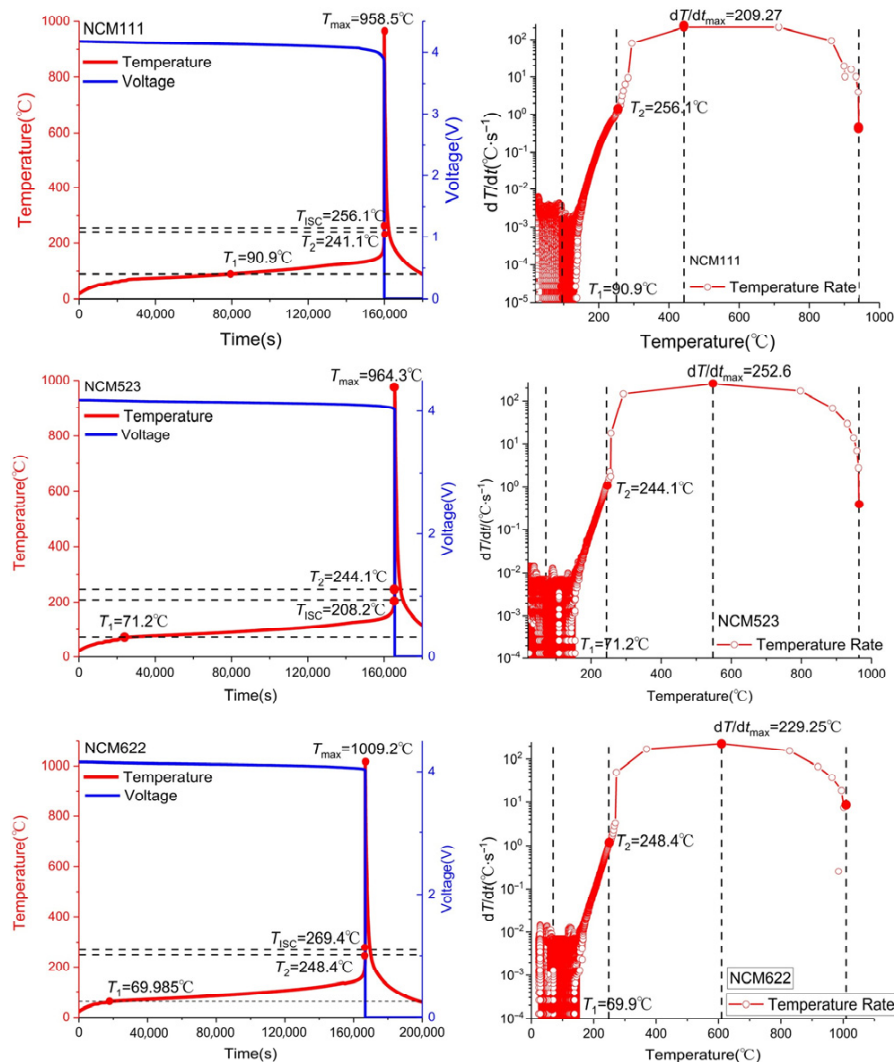


Figure 8. Voltage, temperature and temperature rate curves during thermal runaway for NCM111, NCM523, and NCM622 [71].

3.2.2. Stabilizing Effects and Limitations of Cobalt and Manganese

To counteract the thermal stability challenges associated with high-nickel systems, cobalt (Co) and manganese (Mn) serve critical functions in cathode chemistry. These elements enhance structural integrity, suppress oxygen evolution, postpone thermal runaway onset, and improve thermal robustness—despite their inherent constraints. Cobalt serves as a critical stabilizer for structural thermal stability [55,72]. It effectively suppresses cation mixing between lithium and nickel, preserves the structural integrity of the layered framework, and strengthens the chemical bonds between the transition metal and oxygen layers (TM-O bonds). These combined effects enhance the overall stability of the crystal lattice at elevated temperatures. During thermal runaway events, elemental cobalt mitigates lattice collapse and postpones TR onset. This stabilization mechanism arises from cobalt's ability to suppress oxygen evolution ($O^{2-} \rightarrow O_2$) through crystal lattice stabilization, thereby mitigating risks of vigorous electrolyte reactions. However, cobalt also has some drawbacks. Zhang et al. [48] concluded that the high-valence cobalt ion (Co^{4+}) is unstable at high temperatures and is prone to release energy through reduction reactions and produce O_2 . While manganese ions (Mn^{4+}) similarly undergo valence reduction at high temperatures,

e.g., to Mn³⁺, with the release of oxygen. However, the reduction reaction of cobalt is usually more violent than that of manganese, with relatively faster energy release. This also makes batteries with LMO cathodes generally more thermally stable than LCO batteries. Additionally, as a strategic resource, cobalt's high cost and the ethical concerns associated with its mining are primary drivers behind the pursuit of low-cobalt and cobalt-free cathode materials.

Manganese is recognized as a highly thermostable element that enhances structural robustness and thermal stability in cathode systems [72]. The stabilizing effect of manganese is closely related to the high reversibility of the Mn⁴⁺/Mn³⁺ redox couple. In layered cathode materials such as NCM, manganese predominantly exists in the +4 oxidation state and undergoes reversible reduction to the +3 state during heating. This reversible valence transition effectively mitigates internal stress within the crystal lattice, thereby suppressing abrupt structural collapse and enhancing the structural resilience of the material at elevated temperatures. Nam et al. [61] proposed that manganese in NCM systems contributes to developing a thermally robust spinel configuration, immobilizing Ni³⁺/Co³⁺ species, and suppressing oxygen evolution. Consequently, this reduces oxygen release rates and heat generation, potentially extending the pre-thermal-runaway warning period. Belharouak et al. [49] showed that the oxygen uptake reversibility of low-nickel NCM111 is modulated by the oxidation state of manganese, which keeps the structure reversibly transformed at elevated temperatures, which is the key reason for its thermodynamic stability being superior to that of high-nickel materials. However, manganese dissolution at high temperatures is a concern [76]. Under elevated temperatures and high voltages, Mn³⁺ undergoes a disproportionation reaction ($2\text{Mn}^{3+} \rightarrow \text{Mn}^{2+} + \text{Mn}^{4+}$) or reacts with acidic species (e.g., HF) in the electrolyte to form Mn²⁺. The dissolved Mn²⁺ ions then migrate through the electrolyte and are reductively deposited on the anode surface. The deposited metallic manganese catalyzes the continuous decomposition and thickening of the solid electrolyte interphase (SEI), consuming limited lithium reserves and thereby compromising the protective function of the SEI. An unstable and persistently growing SEI film promotes further side reactions, consequently increasing the propensity for thermal runaway in lithium-ion batteries under abusive conditions. Notably, the absence of manganese in NCA systems contributes to structural instability. Under sustained temperature rise, massive Ni³⁺/Ni⁴⁺-to-Ni²⁺ transformation initiates lattice oxygen release, accelerating heat generation during pre-thermal-runaway phases [61].

3.2.3. Synergies and Optimal Ratios of Chemical Elements

The synergistic interactions among chemical elements hold greater significance than the contribution of any single element; identifying the optimal elemental ratio is critical for enhancing the thermal stability of the cathode material while concurrently increasing its capacity. Utilizing *in situ* high-temperature XRD, Sun et al. [66] demonstrated that the level of thermal stability in NCM cathode materials is primarily governed by the compositional ratio of nickel, cobalt, and manganese. Bak et al. [77] employed mass spectrometry coupled with X-ray diffraction (TR-XRD/MS) to characterize the thermal stability of four distinct charged NMC cathode compositions—NMC433, NMC532, NMC622, and NMC811—during heating to 600 °C. The TR-XRD/MS results revealed that the concentrations of Ni, Co, and Mn exert a substantial influence on structural evolution and oxygen release behavior during heating. Specifically, increased Ni concentration coupled with reduced Co and Mn levels led to a lower phase transition onset temperature and a higher extent of oxygen release. However, NMC532 (Ni:Mn:Co = 5:3:2) exhibits a distinctive advantage: it delivers a high capacity similar to high-nickel cathodes (e.g., NMC811), while maintaining thermal stability on par with low-nickel counterparts (e.g., NMC333, NMC433). This favorable performance origi-

nates from its optimal stoichiometric balance of nickel, manganese, and cobalt, enabling synergistic interplay that leverages the strengths and mitigates the weaknesses of each element. Therefore, solely focusing on either high-nickel or low-nickel compositions is suboptimal. A more favorable trade-off between safety and high energy density can be attained through precise control of elemental composition, as demonstrated by materials like NCM523. Compared with NCM ternary cathodes, NCA ternary cathodes typically feature high-nickel [78] aluminum-containing compositions. Their thermal stability is predominantly governed by nickel concentration, while the influence of specific elemental combinations must also be considered. In the future, high-throughput computation and machine learning can be employed to explore the optimal stoichiometric ratios of elements such as nickel, manganese, and cobalt, thereby balancing capacity and safety. Concurrently, strategies such as bulk doping (e.g., with Zr or Nb) and surface coating should be implemented to simultaneously address the structural instability of high-nickel materials and the issue of manganese dissolution.

3.3. Influence of Thermal Stability on Thermal Runaway Behavior

3.3.1. Centrality and Characterization Parameters of Thermal Stability

The thermal runaway behavior of LIBs is closely linked to cathode material thermal stability [66], which serves as a comprehensive indicator of the material's thermal performance. Thermal runaway initiation stems from multiple factors, with inadequate thermal stability of electrode active materials representing a key contributing factor [67]. Cathode material thermal stability denotes the capacity to maintain structural integrity and property consistency across operational temperature ranges. This attribute collectively manifests the material's structural and compositional attributes, representing the governing intrinsic property that dictates both the initiation propensity and severity of thermal runaway in LIBs. Cathode materials with good thermal stability can maintain the relative stability of their crystal structure and chemical properties within a certain temperature range, effectively inhibiting the occurrence of TR. Conversely, cathodes with inferior thermal stability can precipitate thermal runaway initiation at lower temperatures while liberating greater heat quantities [12], culminating in exacerbated TR hazards. Critical evaluation parameters for thermal stability's impact on TR include: reaction onset temperature (T-onset), total TR heat release (ΔH), and temperature rise rate (dT/dt). These metrics are experimentally derived through thermal analysis techniques.

3.3.2. Measurement of Thermal Stability

Researchers commonly employ differential scanning calorimetry (DSC), accelerating rate calorimetry (ARC), and C80 microcalorimetry to monitor thermal response variations in cells containing different electrode materials [4]. These techniques enable systematic assessment of cathode material thermal stability under thermal stress conditions. Accelerating rate calorimetry (ARC) and differential scanning calorimetry (DSC) represent the primary methodologies employed by research teams to quantify the thermal behavior of lithium-ion electrode materials interacting with salt-free solvents and electrolytes [44,79,80]. Complementing these approaches, the vent sizing package 2 (VSP2) provides an adiabatic technique for evaluating system-level thermal response, with Table 1 summarizing comparative features of these characterization methods.

Table 1. Characterization Methodologies for Cathode Thermal Stability.

	Accelerated Calorimetry (ARC)	Differential Scanning Calorimetry (DSC)	C80 Calorimeter	Vent Sizing Package 2 (VSP2)
Core Principles	Measured under near-adiabatic conditions sample self-heating rate (Heat-Wait-Search mode)	Measurement of the difference in heat flow between the sample and the reference at the programmed temperature	Measurement of sample heat flow in a confined high-pressure cell using a three-dimensional wraparound thermopile	Simultaneous tracking of sample temperature and self-generated pressure changes under near-adiabatic conditions
Test Patterns	Main Insulation Modes	Major isochronous scanning(dynamic), Few constant temperatures (isothermal)	Isometric Scanning(dynamic), Constant temperature (isothermal), Custom programs	Main Insulation Modes
Thermal insulation	Excellent	Inferior	Superior	Excellent
Main output parameters	Temperature-time curve, self-heating rate, adiabatic temperature rise, time to maximum rate	Onset temperature, peak temperature, reaction enthalpy	Temperature-time curve, Onset temperature, peak temperature, reaction enthalpy	Temperature-time curve, Self-heating rate
Vantages	The closest approximation to real thermal runaway conditions provides critical safety parameters	High sensitivity, Measurable phase change	Higher sensitivity than ARC, provides reaction enthalpy data	Simultaneous acquisition of adiabatic temperature rise
Limitations	Relatively low sensitivity to small exotherms	Non-adiabatic results extrapolated to adiabatic conditions need to be modeled	Insulation not as good as ARC/VSP2; maximum pressure/temperature may be slightly lower than ARC/VSP2	Relatively low sensitivity to small exotherms
Representative Applications in Cathode Thermal Behavior Research	Evaluating the thermal behavior of materials under near-realistic thermal runaway conditions, Evaluating the effects of different charging states	Rapid comparison of exothermic onset temperature, peak temperature, and reaction enthalpy for different materials and SOCs	Evaluation of reactions under different states of charge, electrolyte coexistence	Specialized in gas generation during thermal runaway

3.3.3. Thermal Stability of Cathode Materials and Its Impact on Thermal Runaway Behavior

Researchers have conducted systematic assessments of cathode material thermal stability hierarchies using these methodologies, revealing close correlation with their thermal runaway performance. Jiang et al. [81] employed accelerating rate calorimetry (ARC) in EC/DEC solvent to characterize three cathode materials: LiCoO₂, Li[Ni_{0.1}Co_{0.8}Mn_{0.1}]O₂, and LiFePO₄. Comparative analysis revealed autocombustion initiation temperatures of 150 °C, 220 °C, and 310 °C respectively for these materials at a 4.2 V charge state, with LFP demonstrating superior thermal resistance. El Moutchou et al. [58] employed differential scanning calorimetry (DSC) to characterize the thermal behavior of NCM811 and LFP cells under elevated temperatures. The synthesized NMC811 material manifested distinct exothermic events at 212 °C and 259 °C with a cumulative heat release of 94 J/g, whereas LFP exhibited no detectable exothermic activity, demonstrating superior ther-

mal resistance. Zhang et al. [82] characterized the thermal behavior of NCA and NCM811 ternary lithium batteries using coupled differential scanning calorimetry–thermogravimetry and mass spectrometry (DSC-TG-MS). Analysis revealed substantially greater heat generation from NCA during interactions with anode materials or electrolyte compared to NCM811. Overall, NCM811 exhibited reduced thermal runaway propensity and superior practical thermal stability relative to NCA. Collectively, NCM811 demonstrates reduced thermal runaway propensity and enhanced thermal stability relative to NCA in practical applications. Belharouak et al. [49] evaluated the thermal behavior of delithiated $\text{Li}_{0.45}(\text{Ni}_{0.8}\text{Co}_{0.15}\text{Al}_{0.05})\text{O}_2$ versus $\text{Li}_{0.55}(\text{Ni}_{1/3}\text{Co}_{1/3}\text{Mn}_{1/3})\text{O}_2$. Their analysis demonstrated that the manganese-containing composition exhibits: 18% higher reaction onset temperature; 27% reduced exothermic heat release; and enhanced thermodynamic stability relative to the aluminum-modified counterpart. Mendoza-Hernandez et al. [41] employed accelerating rate calorimetry to assess TR characteristics of lithium cobalt oxide (LCO) and lithium manganese oxide (LMO) cathodes under varying SOC conditions. Analysis indicated LCO underwent thermal runaway at 50–120% SOC, while LMO initiated thermal runaway at 75–120% SOC. So LMO has better thermal stability than LCO [48]. The enhanced thermal stability of LCO compared to LMO can be attributed to the reduced tendency of LMO to release oxygen at elevated temperatures [83]. Hu et al. [55] observed via XRD patterns that the diffraction peaks associated with the hexagonal phase (layered structure) progressively diminished as temperature increased, while those corresponding to the cubic phase (spinel) persisted. This observation indicates that $\text{LiNi}_{1/3}\text{Co}_{1/3}\text{Mn}_{1/3}\text{O}_2$ underwent partial reaction initially, and importantly, reveals that LMO exhibits enhanced thermal stability compared to $\text{LiNi}_{1/3}\text{Co}_{1/3}\text{Mn}_{1/3}\text{O}_2$. Jhu et al. [13] employed VSP2 (Vent Sizing Package 2, an accelerated calorimetry technique) to evaluate the thermal stability of charged 18650 Li-ion batteries employing LCO and $\text{Li}(\text{Ni}_{1/3}\text{Co}_{1/3}\text{Mn}_{1/3})\text{O}_2$ cathodes. Their findings demonstrate that LCO batteries exhibit an elevated risk of thermal runaway relative to NCM batteries. Xiang et al. [84] utilized a C80 calorimetry system to assess the thermal stability of various cathode materials: cobalt-based oxides (LiCoO_2 , $\text{LiNi}_{0.8}\text{Co}_{0.15}\text{Al}_{0.05}\text{O}_2$ -NCA, $\text{LiNi}_{1/3}\text{Co}_{1/3}\text{Mn}_{1/3}\text{O}_2$ -NCM333), manganese-based oxide (LiMn_2O_4 -LMO), and olivine-type phosphate (LiFePO_4 -LFP). Among these three categories, the olivine phosphate material (LFP) demonstrated superior thermal stability. Specifically, LFP released negligible heat below 225 °C, with a significant exothermic onset observed at 218 °C, and maintained consistently low heat flow during the entire experiment. Figure 9 presents the C80 heat flow profiles obtained for mixtures of delithiated cathode materials and the electrolyte (1M LiPF_6 in EC/DMC), recorded at a heating rate of 0.2 °C/min. The X-ray diffraction (XRD) patterns characterizing the cathode materials both at room temperature and following heating to 300 °C are displayed in Figure 10 (Note: In Figures 9 and 10, Gen2 denotes $\text{LiNi}_{0.8}\text{Co}_{0.15}\text{Al}_{0.05}\text{O}_2$, L333 denotes $\text{LiNi}_{1/3}\text{Co}_{1/3}\text{Mn}_{1/3}\text{O}_2$, and LFPO denotes LiFePO_4). Based on the comprehensive evaluation, the ranking of thermal stability, from highest to lowest, is: olivine-type LFP > manganese-based LMO > $\text{LiNi}_{1/3}\text{Co}_{1/3}\text{Mn}_{1/3}\text{O}_2$ (NCM333) > cobalt-based LCO > cobalt-based NCA. Zhang et al. [48] argued that, generally, the thermal stability of cathodes in a fully charged state follows the order of LFP > LMO > NMC111 > NCA > LCO. Analysis of existing research on the thermal stability of various cathode materials reveals that LiFePO_4 (LFP) demonstrates superior thermal stability [50]. The established stability ranking is LFP > LiMn_2O_4 (LMO) > $\text{LiNi}_{1/3}\text{Co}_{1/3}\text{Mn}_{1/3}\text{O}_2$ (NMC111) > $\text{LiNi}_{0.8}\text{Co}_{0.1}\text{Mn}_{0.1}\text{O}_2$ (NCM811) > LiCoO_2 (LCO) > $\text{LiNi}_{0.8}\text{Co}_{0.15}\text{Al}_{0.05}\text{O}_2$ (NCA). Notably, materials including LFP and LMO undergo decomposition at elevated temperatures and typically release less energy during this process [19].

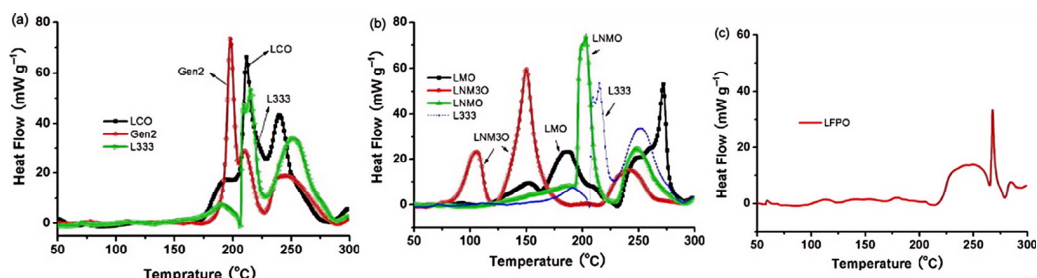


Figure 9. Heat flow profile under coexistence of electrolyte and delithiated cathode material (a) LCO, Gen2 and L333; (b) LMO and L333; (c) LFPO [84].

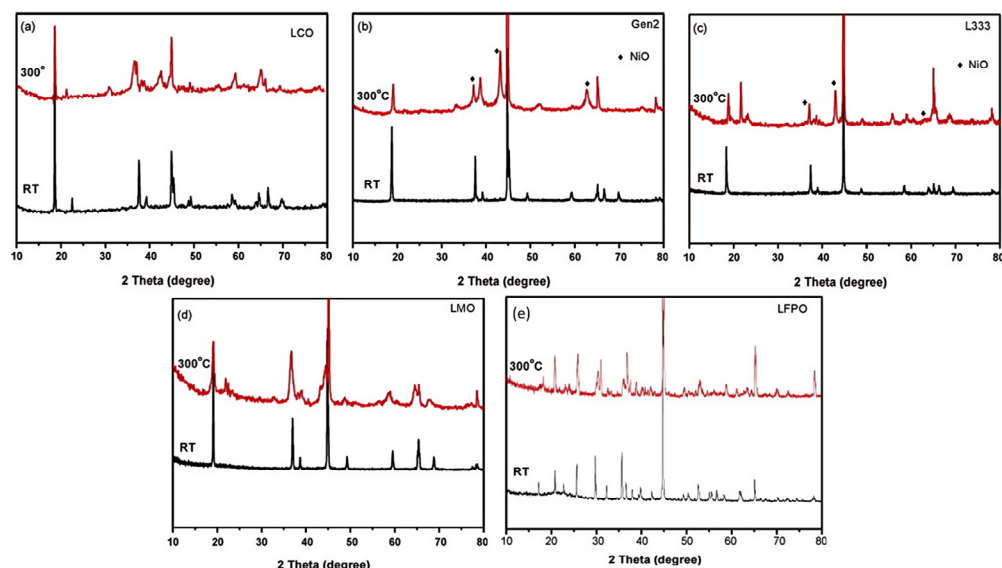


Figure 10. X-ray diffraction profiles characterizing the cathode materials (a) LCO; (b) NCA; (c) NCM; (d) LMO; (e) LFP under ambient conditions and following heating to 300 °C [84].

Generally, a lower onset temperature for self-heating implies that the cathode material initiates heat generation at a reduced threshold. This earlier onset facilitates the initiation of thermal runaway (TR), consequently increasing the associated hazard risk. Furthermore, a large enthalpy change (ΔH) combined with a rapid heating rate (dT/dt) results in substantial energy release occurring at high speed. The heating rate (dT/dt) serves as a more direct indicator of TR intensity. Lamb et al. [19] employed accelerating rate calorimetry (ARC) to evaluate batteries featuring diverse cathode chemistries, sizes, and specifications. Key quantitative findings were derived from the “Temperature vs. heating rate (dT/dt)” profiles normalized to stored energy, presented in Figure 11a,b. Figure 11a reveals that LCO, LMR-NCM (4.4 V), and NCA exhibit pronounced thermal runaway (TR) signatures at their peak heating rates, indicating significant hazards and intense spontaneous reactions. In contrast, LFP and LMO demonstrate markedly lower TR propensity. Figure 11b shows that LCO, NCA, and NCM111 curves initiate rapid ascent near 150 °C. These materials display accelerated exothermic reactions during initial heating, culminating in severe TR events with potentially catastrophic outcomes. This behavior contrasts sharply with the delayed, milder exothermic onset and subsequent TR initiation observed for LFP and LMO.

The effects of state-of-charge (SOC) and testing conditions (e.g., electrolyte composition) must also be accounted for in thermal stability assessments. Elevated SOC promotes oxygen release from the cathode material, consequently elevating the hazard of thermal runaway [41,85]. Additionally, it is important to note that the thermal behavior of nominally identical cathode materials is significantly altered by the electrolyte

environment—including its presence or absence and chemical formulation [81]. The presence of electrolyte typically lowers the exothermic onset temperature of the cathode material compared to its behavior in isolation [49]. Solvent composition also significantly impacts thermal decomposition onset temperatures. For instance, Peng et al. [86] developed a three-dimensional thermal model simulating oven abuse scenarios in lithium-ion batteries. This model was applied to computationally assess the thermal stability and safety of several cathode materials: lithium cobalt oxide (LiCoO_2), lithium nickel cobalt aluminate ($\text{LiNi}_{0.8}\text{Co}_{0.15}\text{Al}_{0.05}\text{O}_2$ —NCA), nickel-rich lithium nickel cobalt manganese oxide ($\text{Li}(\text{Ni}_{1/3}\text{Co}_{1/3}\text{Mn}_{1/3})_{0.9}\text{O}_2$), lithium manganese oxide (LiMn_2O_4 —LMO), and lithium iron phosphate (LiFePO_4 -LFP). Simulations employed an electrolyte containing lithium hexafluorophosphate (LiPF_6) dissolved in a blend of ethylene carbonate (EC), ethyl methyl carbonate (EMC), and dimethyl carbonate (DMC). Figure 12a (where the vertical axis α represents the reaction progress between the cathode material and solvent, with $\alpha = 1$ indicating reaction completion) demonstrates that LMO exhibits a higher decomposition onset temperature than LFP, suggesting superior thermal stability in this specific electrolyte system. However, Figure 12b reveals a substantially higher heat generation rate for LMO compared to LFP. Overall, LFP displays the most favorable safety characteristics. Consequently, authentic battery risk assessment necessitates testing under conditions closely approximating real-world operation. To accurately assess thermal stability in the future, big data can be leveraged to integrate thermal analysis data under varying states of charge (SOC), temperatures, and pressures. Machine learning models, such as neural networks, can then be constructed to enable rapid prediction of critical thermal runaway parameters for cathode materials, including the onset temperature of thermal runaway and the maximum heat release rate. Additionally, establishing unified thermal stability testing standards will enhance the comparability of data across different material systems.

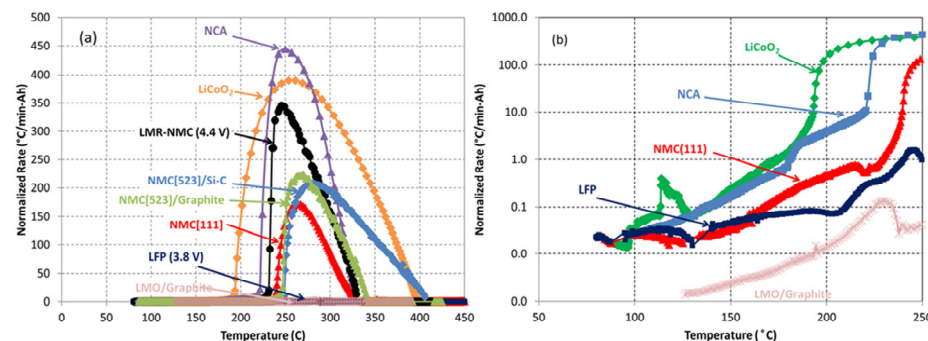


Figure 11. (a,b) Plot of warming rate (dT/dt) versus temperature [19].

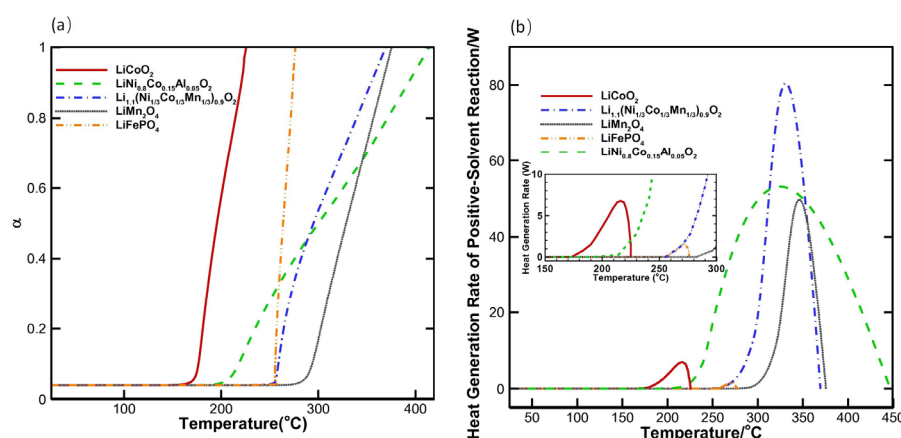


Figure 12. (a) Temperature profiles of different cathode-solvent reactions; (b) heat generation rate curves of different cathode materials [86].

4. Thermal Runaway Behavior of Cathode Materials Under Three Abuses

Thermal runaway (TR) in LIBs typically originates from exposure to extreme conditions, where mechanical, thermal, or electrical abuse activates latent hazards within the cathode materials. Nevertheless, key TR characteristics—including the trigger temperature, intensity (peak temperature, heating rate), and failure manifestations (mass loss)—are primarily governed by the material's inherent structure, chemical composition, and thermal stability. GB 38031 [87], a key battery safety testing standard, specifies three primary thermal abuse test methods: nail penetration, side heating, and overcharging. Most researchers have used these three methods for abuse experiments, and Table 2 shows the key data recorded by the researchers for TR experiments on LIBs with different cathode materials under the three abuses.

Table 2. Summary of thermal runaway experiments of cathode materials under three abuses.

References	Abuse of Conditions	Cathode Materials	Key Parameters					Notes	
			Tmax (°C)	Mass loss (g)	Mass loss ratio (%)	TR trigger time (s)	Time of ejection & fire (s)		
Wei [88]	Mechanical abuse (nail piercing)	NCM 523	964.3	331.3	35.6	1	6	Tmax represents the maximum temperature reached during TR	
	Thermal abuse (heating)	NCM 523	1020	372.1	39.9	180	136		
	Electrical abuse (overcharge)	NCM 523	\	601.1	64.3	4700	165		
Ohneseit [78]	Mechanical abuse (nail piercing)	LFP 21700	Thermal runaway does not occur at SOC of 30%, 50%, and 100% The maximum temperature measured at different locations is 101.9 °C at SOC of 100%						
	Thermal abuse (HWS)	LFP 21700	The onset temperature at 100% SOC is about 124.4 °C Startup thermal runaway temperature of about 256.3 °C, maximum temperature of about 498.6 °C						
	Mechanical abuse (nail piercing)	NCM 21700 (high-nickel)	No thermal runaway at 0% SOC, thermal runaway at 30%, 50%, 100% Maximum temperature at different locations at 100% SOC: 760.3 °C						
	Thermal abuse (HWS)	NCM 21700 (high-nickel)	The SOC is 100%, thermal runaway onset temperature is about 85.5 °C Startup thermal runaway temperature is about 198.0 °C, maximum temperature is about 591.6 °C						
ARC	Mechanical abuse (nail piercing)	NCA 21700 (high-nickel)	No thermal runaway at 0% SOC, thermal runaway at 30%, 50%, 100% Maximum temperature at different locations at 100% SOC: 840.7 °C						
	Thermal abuse (HWS)	NCA 21700 (high-nickel)	The onset temperature at 100% SOC is about 95.3 °C Startup thermal runaway temperature is about 203.1 °C, maximum temperature is about 644.3 °C						

Table 2. Cont.

References	Abuse of Conditions	Cathode Materials	Key Parameters				Notes
An [89]	Mechanical abuse (nail piercing)	LCO	Mass loss (g)	Mass loss ratio (%)	Tmax (°C)	(dT/dt) max (°C/s)	Under 100% SOC 8 mm nail penetration
		LFP	9.55	23.01	About 800	443.9	
		NCM	0	0	54.9	0.124	
		LMO	12.22	26.92	About 700	213.2	
			13.96	22.84	About 520	127.7	
Wang [30]	Electrical abuse (overcharge)	LFP	Mass loss (g)	Mass loss ratio (%)	T onset (°C)	Tmax (°C)	Arrival at the point in time when the TR occurs (S)
		NCM 111	162.8	17.7	112	308	ARC
		NCM 622	309.6	38.7	93	589	
		NCM 811	332.3	42.6	92	629	
			318.9	44.3	93	695	1450
Wang [52]	Electrical abuse (overcharge)	LCO	Mass loss (g)	Mass loss ratio (%)	Tmax (°C)	Fmax (N)	Fmax: peak expansion force
			Charging Rate 0.5C	82.9	65.8	798.2	
			Charging Rate 1C	84.8	67.3	774.6	
			Charging Rate 3C	86.6	68.8	917.2	
		NCM 523	Charging Rate 0.5C	85.7	47.4	679.8	
			Charging Rate 1C	98.3	54.4	680.3	
			Charging Rate 3C	103.7	57.4	683.2	
			Charging Rate 0.5C	32.6	11.4	55.8	
		LFP	Charging Rate 1C	36.5	12.8	127.2	
			Charging Rate 3C	39.1	13.7	252.7	
						7330	
Shen [72]	Thermal abuse	T onset (°C)	T1: Peak temperature at the battery side surface during thermal runaway (°C)	T2: Maximum temperature recorded on the external battery surface during the thermal runaway event (°C)	T3: Maximum temperature observed on the battery heating surface throughout thermal runaway (°C)	T4: Peak average temperature attained during the thermal runaway process (°C)	adiabatic explosion chamber (AEC) T onset: TR onset temperature.
		LFP	184.0	170.9	306.6	559.2	302.1
		NCM 523	142.7	370.6	589.3	695.5	549.3
		NCM 622	140.8	555.9	504.8	600.6	597.1

Table 2. Cont.

References	Abuse of Conditions	Cathode Materials	Key Parameters				Notes
		NCM 811	135.6	564.2	767.6	826.1	762.8
		NCM 9 0.5 0.5	130.6	843.5	903.7	943.9	842.1
Jhu [13]	Thermal abuse		T0 (°C)	Tmax (°C)	(dT/dt) max (°C/min)	ΔH (kJ)	VSP2
		LCO	131.5	708.8	54,090.7	18.9	
		NCM 111	175.4	665.6	15,213.4	14.9	

In mechanical abuse scenarios, nail penetration can induce immediate physical contact between the positive and negative current collectors, resulting in simultaneous short-circuit events across all cell layers [26]. The fundamental mechanism of thermal runaway initiated by nail penetration involves internal short-circuiting and localized overheating. The hazard potential escalates with reduced structural integrity of the cathode material and a lower onset temperature for oxygen evolution. Elevated state of charge (SOC) correlates with diminished thermal stability in Li-ion batteries. Specifically, higher SOC levels reduce the onset temperature while elevating the maximum temperature reached during thermal runaway events [90]. Based on the experimental findings of Ohnesoit [78] and An [89], LFP cells did not experience thermal runaway under nail penetration conditions, even at 100% SOC. This enhanced safety characteristic demonstrates that olivine-structured LFP exhibits superior structural stability among cathode materials, with virtually no oxygen release observed. The peak temperatures during thermal runaway of NCM, NCA, and LCO were very high, and the peak temperature of LCO reached about 800 °C, and the laminated structure of the anode materials The oxygen release is much larger than that of the olivine-structured cathode material. Mao et al. [91] systematically evaluated the thermal response characteristics of lithium-ion batteries (LIBs) featuring LCO, NMC622, and LFP cathodes at identical capacities under mechanical intrusion scenarios (nail penetration). Experimental results demonstrated that NMC622 cells exhibited the poorest internal short-circuit tolerance, with LCO cells displaying intermediate vulnerability and LFP cells showing superior robustness. Post-abuse analysis revealed minimal structural compromise in LFP material following both penetration and crushing events. Conversely, significant mechanical damage to particles and crystal lattices was observed in both LCO and NMC622 materials after nail intrusion, with LCO specimens exhibiting particularly pronounced degradation. Based on nail penetration tests at 100% SOC, An et al. [89] determined that thermal runaway severity followed the hierarchy: LCO > NCM > LMO > LFP.

Under thermal abuse, heating triggers thermal runaway by initiating a chain reaction, and the nickel content is negatively correlated with the temperature of oxygen release. Experimental data from Shen et al. [72] confirms that LFP cathodes exhibit superior thermal runaway initiation temperatures and reduced peak average temperatures during thermal events relative to NCM systems. Furthermore, LFP maintains enhanced thermal stability versus both NCM and NCA materials at 100% SOC. At high temperatures, the strong P-O bonding of LFP inhibits oxygen escape, whereas lattice oxygen is released during the high-temperature phase transition of the laminated cathode (NCM/NCA), and the more nickel content, the more unstable the material is at high temperatures. In thermal abuse, NMC batteries with high-nickel have lower thermal runaway onset temperatures than NCA and LFP batteries when SOC is 100%, indicating that NCM cathode materials

with high-nickel are less resistant and thermally stable than NCA and LFP under thermal abuse. This instability arises from phase transitions and oxygen release in high-nickel NCM chemistries during heating. Concurrently, elevated energy density levels promote intensified exothermic behavior inside the cell, liberating substantial thermal energy [92]. However, probably because NCA cathode materials can decompose suddenly [40], NCA batteries enter thermal runaway slightly earlier than high-nickel NMC batteries.

During electrical abuse scenarios, thermal runaway initiation primarily stems from oxygen liberation during lattice collapse. Material instability intensifies with progressive delithiation, substantially elevating anode hazard risks. Experimental investigations by Wang et al. [30,52] demonstrate that LFP batteries exhibit markedly elevated thermal runaway initiation temperatures alongside reduced peak temperatures, mass depletion, and reaction rates during thermal events when benchmarked against NCM and LCO battery systems. The thermal runaway responses of LCO and NCM with a layered structure are comparable. During overcharge conditions, anode stability deteriorates in the delithiated state, where laminar structures exhibit inferior phase integrity compared to olivine configurations, accelerating lattice collapse. This structural failure coincides with oxygen evolution, with LFP cells generating substantially lower oxygen volumes than LCO and NCM counterparts. Consequently, LFP demonstrates superior thermal stability and enhanced safety performance.

Due to their distinct intrinsic characteristics, lithium-ion batteries employing different cathode materials exhibit notable differences in ignition and combustion behavior during thermal runaway. Layered structure materials such as LCO, NCA, and high-nickel NCM release substantial amounts of oxygen, which react vigorously with the electrolyte. This process is typically accompanied by intense flames and jetting phenomena, along with the generation of large volumes of flammable gases, thereby elevating the risk of explosion. The thermal runaway behavior of NCA under thermal abuse conditions is shown in Figure 13a–f [93]. In contrast, LFP batteries typically exhibit no visible flames or only weak flames during thermal runaway. As shown in Figure 13g [94], which captures the macroscopic behavior of an LFP battery under mechanical abuse, the cell initially deforms, followed by the release of significant white smoke and casing rupture, while overall maintaining a relatively intact appearance. The thermal runaway behavior of LMO batteries lies intermediate between that of layered cathode materials and LFP. An et al. [89] investigated the combustion behavior and post-test appearance of lithium-ion batteries with different cathode materials subjected to nail penetration with an 8 mm steel needle at 100% SOC. They observed that NCM, LCO, and LMO batteries exhibited similar behavior: the cells swelled severely at the moment of penetration, accompanied by the release of a small amount of grayish-white smoke. Subsequently, significant sparking occurred at the penetration site along with the generation of abundant grayish-white smoke, followed by a violent fire that lasted approximately 20 s before extinguishing. Specifically, the NCM and LCO batteries suffered severe structural damage. In contrast, the LMO batteries maintained a relatively intact structure, with only deformation and bulging observed in the electrode layers. The LFP batteries showed no significant abnormal phenomena. In an overcharging study on NCM, LFP, and LCO lithium-ion batteries, Wang et al. [52] reported distinct thermal runaway behaviors among the three chemistries. The NCM cell showed no significant swelling in the initial stage. Subsequently, gas generation inside the cell led to noticeable swelling of the surface, followed by severe bulging accompanied by the release of high-temperature smoke and intense sparking. The combination of ejected flammable electrolytes, oxygen, and sparks instantly triggered a violent jet fire with a peak flame temperature of 740.4 °C. The LCO battery exhibited significant similarities to the NCM battery in thermal runaway behavior, with the difference that the LCO cell went through

expansion–contraction cycles. In contrast, although the LFP battery experienced severe internal swelling that ruptured the sealing edges due to high internal pressure, no sparking, explosion, or ignition was observed during the process, demonstrating a lower risk of thermal runaway compared to the layered oxide cathodes.

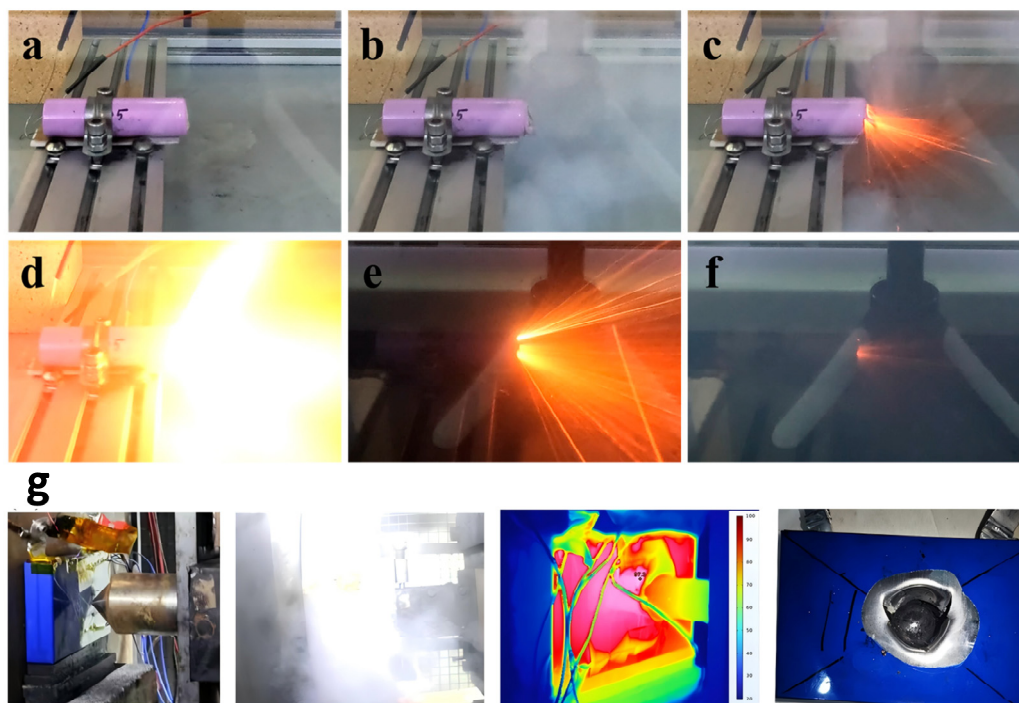


Figure 13. (a–f) Sequence of thermal runaway processes in NCA lithium-ion batteries under thermal abuse [93]. (g) Experimental photographs and infrared images of LFP cells under mechanical abuse [94].

In summary, LFP demonstrates significantly milder responses under various abuse conditions compared to other cathode materials, exhibiting the highest structural stability, minimal oxygen release during thermal runaway, and superior thermal stability, thus presenting the lowest risk of thermal runaway. Additionally, LFP batteries generally do not ignite during thermal runaway events and sustain the least structural damage post-failure. NCM523 cathode material exhibits the shortest thermal runaway initiation time under mechanical abuse scenarios, with its layered structure demonstrating the highest susceptibility to mechanical damage. This cathode chemistry shows the poorest safety performance during nail penetration events. Under electrical abuse conditions, it incurs the most substantial mass loss and highest mass depletion rates while manifesting the most severe degradation during overcharge situations. Both layered and spinel cathode materials are prone to combustion. Cathode material safety performance generally follows this descending hierarchy: LFP > LMO > NCM > LCO [95]. Among commercial lithium-ion chemistries, LFP batteries consistently demonstrate the lowest thermal runaway propensity. Understanding the differences in fire behavior among lithium-ion batteries with different cathode materials is crucial for formulating targeted safety strategies for battery systems. Future efforts should focus on developing artificial intelligence-based early warning algorithms that integrate multiple signals—thermal, electrical, and gas-related—and on establishing multi-scale models coupled with electrochemical, thermal, and chemical processes to accurately predict battery behavior under complex abuse scenarios.

5. Impact of Cathode Materials on System-Level Safety

The preceding sections have discussed the differences in thermal runaway behavior among lithium-ion batteries with different cathode materials at the single-cell level under abuse conditions. In practical battery packs or energy storage systems, however, the thermal runaway of a single cell represents only the initiation of a safety incident. It is the ensuing thermal runaway propagation and consequent system-level hazards—such as fire spread and gas explosions—that primarily lead to catastrophic consequences [96]. Serving as the primary source of thermal runaway energy, the intrinsic properties of cathode materials critically govern both the rate of module-level propagation and the severity of system-level hazards.

5.1. Role of Cathode Materials in Module-Level Thermal Runaway Propagation

Thermal runaway propagates through heat transfer modes such as heat conduction, heat convection, and thermal radiation from a single cell, thereby triggering thermal runaway in adjacent cells and causing fires [97]. The propagation of thermal runaway within a module fundamentally involves the energy released by a single cell in thermal runaway heating adjacent cells to their critical temperature. In this process, the cathode material governs both the intensity and rate of thermal runaway propagation. Different cathode materials exhibit distinct thermal runaway onset temperatures. The variation in onset temperature directly affects the propagation dynamics, where a higher triggering temperature prolongs the average cell-to-cell propagation time [98]. Additionally, layered high-nickel cathode materials such as NCA, NCM811, and LCO exhibit high heat release rates (dT/dt) and total heat release (ΔH) during thermal runaway. When thermal runaway occurs in these materials, the failing cell can transfer substantial energy to adjacent cells within a very short period, significantly reducing the time required for neighboring cells to reach their critical temperature and resulting in extremely rapid propagation. In contrast, the mild thermal runaway characteristics of LFP cells largely suppress the tendency for propagation, and in many well-designed systems, the propagation can even be arrested. Beyond heat conduction, the intense flames and ejecta generated by reactions between oxygen released from cathode material decomposition and the electrolyte also promote module-level thermal runaway propagation. The vigorous jet flames triggered during thermal runaway in layered cathode materials like LCO and NCA produce intense local thermal radiation and convective heating, simultaneously affecting multiple adjacent cells and drastically accelerating the propagation process. Moreover, the chemical composition of cathode materials significantly influences thermal runaway propagation. Li et al. [99] investigated the thermal runaway propagation characteristics of lithium-ion batteries with NCM111, NCM523, and NCM622 cathodes. Their results demonstrate that as the nickel content in the cathode material increases, the risk of thermal runaway propagation under thermal abuse conditions intensifies, thereby increasing the likelihood of jet fires. In contrast, LFP cells typically exhibit no open flames or only weak flames, fundamentally eliminating this propagation pathway.

5.2. Modulation of System-Level Hazard Characteristics by Cathode Materials

Once thermal runaway propagates within a module, the risks escalate further. System-level thermal runaway accidents typically manifest through two hazardous pathways: gas explosions and large-scale fires [96]. During thermal runaway, substantial amounts of flammable gases such as H_2 , CO, and CH_4 are generated [100]. The cathode material influences the yield and composition of flammable gases through its decomposition pathways and reactions with the electrolyte. Layered cathode materials with high energy density typically generate larger amounts of flammable gases during intense side reactions.

During the propagation of thermal runaway, a large quantity of flammable gases is continuously released and diffused in the fluid domain. When these gases accumulate in a closed or semi-closed space and meet the three elements of combustion (i.e., combustible substance, oxidizer, and ignition source), an explosion accident may be triggered [96]. Although LFP cells also produce flammable gases, their total gas volume and combustion intensity are generally significantly lower than those of layered cathode materials. It is noteworthy that, in their thermal runaway experiments comparing LFP and NCM batteries, Wang et al. [100] observed that LFP cells generated a larger amount of H₂ than NCM cells. Given the low explosion limit of H₂, this finding suggests that the vented gas mixture from LFP batteries may potentially pose a greater hazard than that from NCM batteries. Moreover, the reactive oxygen species released from cathode materials fundamentally alter the nature of the fire. In the case of layered cathode materials, thermal runaway fires involve hybrid combustion of the electrolyte and lattice oxygen, which markedly reduces the effectiveness of conventional fire suppression methods using nitrogen or carbon dioxide since the battery internally maintains a sustained oxygen supply. This characteristic significantly increases the difficulty and duration of system-level firefighting. In contrast, LFP materials release virtually no oxygen, and their combustion primarily depends on external air, making traditional extinguishing approaches considerably more effective.

In summary, cathode materials serve not only as the cornerstone of cell energy density but also as the primary driver of module-level propagation, while critically modulating system-level hazards such as explosions and fires. Consequently, the pursuit of next-generation lithium-ion batteries with enhanced safety must place equal emphasis on the intrinsic thermal safety and electrochemical performance of cathode materials. Future efforts should focus on developing full-scale models capable of accurately describing the entire chain of events—from cell failure to module-level propagation and ultimately to system-level fire and explosion hazards. Such models are essential to elucidate the amplifying effect of cathode material properties on macroscopic disasters and to provide theoretical tools for system-level safety design and emergency preparedness.

6. Summary and Outlook

6.1. Summary

This review systematically examines recent advances in the thermal runaway behavior of lithium-ion batteries, with the main conclusions including:

1. During thermal runaway events, cathode materials act as primary contributors. Oxygen liberated through their thermal decomposition serves as a key accelerator of the runaway process; greater oxygen evolution is directly proportional to intensified exothermic reactions. With LFP cathodes exhibiting negligible oxygen evolution, they demonstrate significantly reduced hazard potential compared to alternative cathode chemistries.
2. Crystal configuration fundamentally governs the inherent thermal resilience of cathode materials, with structural stability typically ranking: olivine > spinel > layered. The strong covalent bonding of PO₄ tetrahedra in the structure of olivine locks oxygen with excellent thermal stability. The (PO₄)³⁻ polyanion can convert the heat released from oxygen into phase transition energy and realize flame retardancy. Delithiation-induced structural collapse in layered cathode materials is the root cause of high risk, and the layered structure requires phase transition modulation to compensate for the lack of structural stability. Development of the Co₃O₄ spinel phase within NCM cathodes plays a critical role in mitigating severe thermal runaway propagation.
3. NCM with high-nickel content is less thermally stable than low-nickel materials, and NCM with low-nickel content does not have the high capacity of high-nickel materials.

Balancing thermal stability and high capacity, and exploring the optimal ratio between nickel, cobalt, and manganese chemical elements is a better method than adjusting the content of a single nickel element.

4. Cathode materials exhibit an inherent thermal resilience hierarchy: LFP > LMO > NCM111 > NCM811 > LCO > NCA. However, this hierarchy is substantially modulated by state-of-charge (SOC) levels and operational environmental conditions.
5. Under three types of abuse conditions, the inherent risks of cathode materials are activated. LFP with an olivine structure demonstrates the highest safety performance under mechanical, electrical, and thermal abuse, typically exhibiting no open flames or only weak flames during thermal runaway. In contrast, layered structure materials exhibit lower onset temperatures of thermal runaway than LFP under all three abuse conditions, along with higher maximum temperatures during the process. They are also accompanied by intense jetting flames and the generation of substantial amounts of flammable gases, resulting in a significantly higher fire risk.
6. The influence of cathode materials spans multiple scales. At the module level, highly reactive layered materials significantly accelerate thermal runaway propagation. At the system level, the released reactive oxygen species and substantial amounts of flammable gases increase fire suppression difficulty and the risk of gas cloud explosions, respectively, thereby dictating the safety design strategies and costs of battery systems.

6.2. Outlook

This review systematically summarizes the intrinsic connection between cathode materials and thermal runaway behavior in lithium-ion batteries. Although significant progress has been made in understanding this relationship, numerous challenges remain in achieving battery systems that simultaneously deliver high safety and high energy density. Future research is expected to achieve breakthroughs in the following directions. First, developing intrinsically safe novel cathode materials is crucial, including suppressing oxygen release and stabilizing the layered framework through bulk doping, surface coating, and structural design, along with actively exploring cobalt-free or low-cobalt material systems. Second, constructing intelligent safety warning models based on multi-physics coupling is essential. This requires integrating multiple signals—electrical, thermal, mechanical, and gas—and utilizing big data and machine learning technologies to achieve early, accurate prediction and intelligent management of thermal runaway. Finally, research should adopt a multi-scale perspective—from material to cell, module, and system levels—to elucidate the propagation and amplification effects of cathode material properties across larger scales, thereby providing a theoretical foundation for battery safety design.

Author Contributions: Conceptualization, Y.Y., Y.G. and Y.M.; methodology, Y.Y., Y.G., Y.M., Y.L. and X.R.; validation, Y.Y. and Y.G.; investigation, Y.Y. and Y.M.; resources, Y.G.; data curation, Y.Y.; writing—original draft preparation, Y.Y.; writing—review and editing, Y.G., Y.Y., X.R. and Y.L.; visualization, Y.Y. and Y.M.; supervision, Y.G. All authors have read and agreed to the published version of the manuscript.

Funding: This research was funded by the Ningxia Natural Science Foundation, grant number No. 2024AAC03190; the Ningxia Composite Manufacturing System Engineering Technology Research Center, grant number No. 2023GCJS008; and the Ningxia Leading Talents in Science and Technology Program, grant number No. 2024GKLRLX03.

Data Availability Statement: No new data were created or analyzed in this study.

Conflicts of Interest: The authors declare no conflicts of interest.

Abbreviations

The following abbreviations are used in this manuscript:

LIB	Lithium-ion battery
TR	Thermal runaway
SEI	Solid-electrolyte interphase
ARC	Accelerating rate calorimetry
LiFePO ₄ (LFP)	Lithium iron phosphate
LiMn ₂ O ₄ (LMO)	Lithium manganate
LiCoO ₂ (LCO)	Lithium cobaltate
NMC	Lithium-nickel-manganese-cobalt oxide
NCA	Lithium-nickel-cobalt-aluminum oxide
Ni	Nickel
ISC	Internal short circuit
SEI	Solid electrolyte interphase
CO ₂	Carbon dioxide
O ₂	Oxygen
C ₂ H ₄	Ethylene
DSC	Differential scanning calorimetry
XRD	X-ray diffraction
RT	Room temperature
Co	Cobalt
Mn	Manganese
T-onset	Reaction onset temperature
ΔH	Total thermal runaway heat release
dT/dt	Temperature rise rate
VSP2	Vent sizing package 2
SOC	State of charge
HWS	Heating-waiting-search
Tmax	Maximum temperature reached during TR
Fmax	Peak expansion force
AEC	Adiabatic explosion chamber
T ₀	Initial exothermic temperature

References

1. Ouyang, D.X.; Chen, M.Y.; Liu, J.H.; Wei, R.C.; Weng, J.W.; Wang, J. Investigation of a commercial lithium-ion battery under overcharge/over-discharge failure conditions. *RSC Adv.* **2018**, *8*, 33414–33424. [[CrossRef](#)]
2. Ouyang, D.; Weng, J.; Chen, M.; Wang, J. What a role does the safety vent play in the safety of 18650-size lithium-ion batteries? *Process Saf. Environ. Prot.* **2022**, *159*, 433–441. [[CrossRef](#)]
3. Jia, Z.; Qin, P.; Li, Z.; Wei, Z.; Jin, K.; Jiang, L.; Wang, Q. Analysis of gas release during the process of thermal runaway of lithium-ion batteries with three different cathode materials. *J. Energy Storage* **2022**, *50*, 104302. [[CrossRef](#)]
4. Jhu, C.-Y.; Wang, Y.-W.; Shu, C.-M.; Chang, J.-C.; Wu, H.-C. Thermal explosion hazards on 18650 lithium ion batteries with a VSP2 adiabatic calorimeter. *J. Hazard. Mater.* **2011**, *192*, 99–107. [[CrossRef](#)] [[PubMed](#)]
5. Cai, T.; Stefanopoulou, A.G.; Siegel, J.B. Modeling Li-Ion Battery Temperature and Expansion Force during the Early Stages of Thermal Runaway Triggered by Internal Shorts. *J. Electrochem. Soc.* **2019**, *166*, A2431. [[CrossRef](#)]
6. Talele, V.; Morali, U.; Patil, M.S.; Panchal, S.; Fraser, R.; Fowler, M.; Thorat, P.; Gokhale, Y.P. Computational modelling and statistical evaluation of thermal runaway safety regime response on lithium-ion battery with different cathodic chemistry and varying ambient condition. *Int. Commun. Heat Mass Transf.* **2023**, *146*, 106907. [[CrossRef](#)]
7. Huang, Z.; Liu, J.; Zhai, H.; Wang, Q. Experimental investigation on the characteristics of thermal runaway and its propagation of large-format lithium ion batteries under overcharging and overheating conditions. *Energy* **2021**, *233*, 121103. [[CrossRef](#)]
8. Zhu, Q.; Liang, K.F.; Zhou, X. Research on Thermal Runaway Characteristics of High-Capacity Lithium Iron Phosphate Batteries for Electric Vehicles. *World Electr. Veh. J.* **2024**, *15*, 147. [[CrossRef](#)]
9. Liu, P.; Li, Y.; Mao, B.; Chen, M.; Huang, Z.; Wang, Q. Experimental study on thermal runaway and fire behaviors of large format lithium iron phosphate battery. *Appl. Therm. Eng.* **2021**, *192*, 116949. [[CrossRef](#)]

10. Lei, B.; Zhao, W.; Ziebert, C.; Uhlmann, N.; Rohde, M.; Seifert, H.J. Experimental Analysis of Thermal Runaway in 18650 Cylindrical Li-Ion Cells Using an Accelerating Rate Calorimeter. *Batteries* **2017**, *3*, 14. [[CrossRef](#)]
11. Maleki, H.; Howard, J.N. Role of the cathode and anode in heat generation of Li-ion cells as a function of state of charge. *J. Power Sources* **2004**, *137*, 117–127. [[CrossRef](#)]
12. Liu, X.; Ren, D.S.; Hsu, H.J.; Feng, X.N.; Xu, G.L.; Zhuang, M.H.; Gao, H.; Lu, L.G.; Han, X.B.; Chu, Z.Y.; et al. Thermal Runaway of Lithium-Ion Batteries without Internal Short Circuit. *Joule* **2018**, *2*, 2047–2064. [[CrossRef](#)]
13. Jhu, C.-Y.; Wang, Y.-W.; Wen, C.-Y.; Shu, C.-M. Thermal runaway potential of LiCoO_2 and $\text{Li}(\text{Ni}_{1/3}\text{Co}_{1/3}\text{Mn}_{1/3})\text{O}_2$ batteries determined with adiabatic calorimetry methodology. *Appl. Energy* **2012**, *100*, 127–131. [[CrossRef](#)]
14. Tian, Z.C.; Yu, H.; Zhang, Z.; Xu, X.J. Performance Improvements of Cobalt Oxide Cathodes for Rechargeable Lithium Batteries. *ChemBioEng Rev.* **2018**, *5*, 111–118. [[CrossRef](#)]
15. Rodrigues, M.T.F.; Babu, G.; Gullapalli, H.; Kalaga, K.; Sayed, F.N.; Kato, K.; Joyner, J.; Ajayan, P.M. A materials perspective on Li-ion batteries at extreme temperatures. *Nat. Energy* **2017**, *2*, 17108. [[CrossRef](#)]
16. Galushkin, N.E.; Yazvinskaya, N.N.; Galushkin, D.N. Causes and mechanism of thermal runaway in lithium-ion batteries, contradictions in the generally accepted mechanism. *J. Energy Storage* **2024**, *86*, 111372. [[CrossRef](#)]
17. Manthiram, A.; Knight, J.C.; Myung, S.T.; Oh, S.M.; Sun, Y.K. Nickel-Rich and Lithium-Rich Layered Oxide Cathodes: Progress and Perspectives. *Adv. Energy Mater.* **2016**, *6*, 1501010. [[CrossRef](#)]
18. Wang, Q.S.; Sun, J.H.; Chen, X.F.; Chu, G.Q.; Chen, C.H. Effects of solvents and salt on the thermal stability of charged LiCoO_2 . *Mater. Res. Bull.* **2009**, *44*, 543–548. [[CrossRef](#)]
19. Lamb, J.; Torres-Castro, L.; Hewson, J.C.; Shurtz, R.C.; Preger, Y. Investigating the Role of Energy Density in Thermal Runaway of Lithium-Ion Batteries with Accelerating Rate Calorimetry. *J. Electrochem. Soc.* **2021**, *168*, 060516. [[CrossRef](#)]
20. Ouyang, D.; Chung, Y.-H.; Liu, J.; Bai, J.; Zhou, Y.; Chen, S.; Wang, Z.; Shu, C.-M. Characteristics and mechanisms of as well as evaluation methods and countermeasures for thermal runaway propagation in lithium-ion batteries. *Prog. Energy Combust. Sci.* **2025**, *108*, 101209. [[CrossRef](#)]
21. Ouyang, D.; Liu, X.; Liu, B.; Wang, Z. An experimental investigation on thermal runaway features of lithium-ion battery modules under tunnel scenarios. *Int. Commun. Heat Mass Transf.* **2025**, *164*, 108922. [[CrossRef](#)]
22. He, X.; Hu, Z.; Restuccia, F.; Yuan, H.; Rein, G. Self-heating ignition of large ensembles of Lithium-ion batteries during storage with different states of charge and cathodes. *Appl. Therm. Eng.* **2021**, *197*, 117349. [[CrossRef](#)]
23. Yan, W.H.; Huang, W.X.; Yang, Y.; Wei, Z.W.; Zhen, H.S.; Lin, Y. Research on overcharge mitigations and thermal runaway risk of 18650 lithium-ion batteries. *J. Energy Storage* **2025**, *120*, 116372. [[CrossRef](#)]
24. Liu, S.T.; Li, Y.; Han, D.C.; Sun, J.L.; Wang, H.B.; Li, Y. Thermal runaway procedure and residue analysis of LiFePO_4 batteries with different charging states under nail penetrating. *J. Appl. Electrochem.* **2024**, *54*, 1485–1500. [[CrossRef](#)]
25. Zhou, Z.; Li, M.; Zhou, X.; Li, L.; Ju, X.; Yang, L. Investigating thermal runaway triggering mechanism of the prismatic lithium iron phosphate battery under thermal abuse. *Renew. Energy* **2024**, *220*, 119674. [[CrossRef](#)]
26. E, J.; Xiao, H.; Tian, S.; Huang, Y. A comprehensive review on thermal runaway model of a lithium-ion battery: Mechanism, thermal, mechanical, propagation, gas venting and combustion. *Renew. Energy* **2024**, *229*, 120762. [[CrossRef](#)]
27. Zhang, Z.; Ji, C.; Wang, Y. Failure Mechanism and Thermal Runaway in Batteries during Micro-Overcharge Aging at Different Temperatures. *Materials* **2024**, *17*, 2125. [[CrossRef](#)]
28. Adanouj, I.; Kriston, Á.; Ruiz, V.; Pfarrang, A. Identification and Quantification of Decomposition Mechanisms in Lithium-Ion Batteries; Input to Heat Flow Simulation for Modeling Thermal Runaway. *JoVE* **2022**, e62376. [[CrossRef](#)]
29. Chen, A.; Sahin, R.; Ströbel, M.; Kottke, T.; Hecker, S.; Fill, A. A Comprehensive Model and Experimental Investigation of Venting Dynamics and Mass Loss in Lithium-Ion Batteries Under a Thermal Runaway. *Batteries* **2025**, *11*, 96. [[CrossRef](#)]
30. Wang, Z.P.; Yuan, J.; Zhu, X.Q.; Wang, H.; Huang, W.; Wang, Y.T.; Xu, S.Q. Overcharge-to-thermal-runaway behavior and safety assessment of commercial lithium-ion cells with different cathode materials: A comparison study. *J. Energy Chem.* **2021**, *55*, 484–498. [[CrossRef](#)]
31. Yuan, Y.; Ma, Q.; Zhang, X.Q.; Zhang, F.; Song, X.N.; Xin, H.C.; Zhu, G.R.; Zhang, H.Z. Influence of cathode materials on thermal characteristics of lithium-ion batteries. *Front. Chem.* **2024**, *12*, 1324840. [[CrossRef](#)]
32. Li, T.; Jiao, Y. Revealing the Thermal Runaway Behavior of Lithium Iron Phosphate Power Batteries at Different States of Charge and Operating Environment. *Int. J. Electrochem. Sci.* **2022**, *17*, 221030. [[CrossRef](#)]
33. Luo, W.; Zhang, S.; Gao, Y.; Shen, C. Review of mechanisms and detection methods of internal short circuits in lithium-ion batteries. *Ionics* **2025**, *31*, 3945–3964. [[CrossRef](#)]
34. Perea, A.; Paolella, A.; Dubé, J.; Champagne, D.; Mauger, A.; Zaghib, K. State of charge influence on thermal reactions and abuse tests in commercial lithium-ion cells. *J. Power Sources* **2018**, *399*, 392–397. [[CrossRef](#)]
35. Chen, Y. Recent advances of overcharge investigation of lithium-ion batteries. *Ionics* **2022**, *28*, 495–514. [[CrossRef](#)]
36. Zhong, H.Y.; Zhong, Q.D.; Yang, J.; Zhong, S.W. Thermal behavior and failure mechanisms of 18650 lithium ion battery induced by overcharging cycling. *Energy Rep.* **2022**, *8*, 7286–7296. [[CrossRef](#)]

37. Zheng, S.Q.; Wang, L.; Feng, X.N.; He, X.M. Probing the heat sources during thermal runaway process by thermal analysis of different battery chemistries. *J. Power Sources* **2018**, *378*, 527–536. [CrossRef]
38. Mao, N.; Zhang, T.; Wang, Z.R.; Gadkari, S.; Wang, J.L.; He, T.F.; Gao, T.F.; Cai, Q. Revealing the thermal stability and component heat contribution ratio of overcharged lithium-ion batteries during thermal runaway. *Energy* **2023**, *263*, 125786. [CrossRef]
39. Lee, K.-S.; Myung, S.-T.; Kim, D.-W.; Sun, Y.-K. AlF₃-coated LiCoO₂ and Li[Ni_{1/3}Co_{1/3}Mn_{1/3}]O₂ blend composite cathode for lithium ion batteries. *J. Power Sources* **2011**, *196*, 6974–6977. [CrossRef]
40. Barkholtz, H.M.; Preger, Y.; Ivanov, S.; Langendorf, J.; Torres-Castro, L.; Lamb, J.; Chalamala, B.; Ferreira, S.R. Multi-scale thermal stability study of commercial lithium-ion batteries as a function of cathode chemistry and state-of-charge. *J. Power Sources* **2019**, *435*, 226777. [CrossRef]
41. Mendoza-Hernandez, O.S.; Ishikawa, H.; Nishikawa, Y.; Maruyama, Y.; Umeda, M. Cathode material comparison of thermal runaway behavior of Li-ion cells at different state of charges including over charge. *J. Power Sources* **2015**, *280*, 499–504. [CrossRef]
42. Li, Y.; Liu, X.; Wang, L.; Feng, X.N.; Ren, D.S.; Wu, Y.; Xu, G.L.; Lu, L.G.; Hou, J.X.; Zhang, W.F.; et al. Thermal runaway mechanism of lithium-ion battery with LiNi_{0.8}Mn_{0.1}Co_{0.1}O₂ cathode materials. *Nano Energy* **2021**, *85*, 105878. [CrossRef]
43. Hou, X.Y.; Kimura, Y.; Tamenori, Y.; Nitta, K.; Yamagishi, H.; Amezawa, K.; Nakamura, T. Thermodynamic Analysis Enables Quantitative Evaluation of Lattice Oxygen Stability in Li-Ion Battery Cathodes. *ACS Energy Lett.* **2022**, *7*, 1687–1693. [CrossRef]
44. Röder, P.; Stiaszny, B.; Ziegler, J.C.; Baba, N.; Lagaly, P.; Wiemhöfer, H.-D. The impact of calendar aging on the thermal stability of a LiMn₂O₄–Li(Ni_{1/3}Mn_{1/3}Co_{1/3})O₂/graphite lithium-ion cell. *J. Power Sources* **2014**, *268*, 315–325. [CrossRef]
45. Ding, Y.; Li, Y.; Xu, R.Y.; Han, X.; Huang, K.; Ke, X.X.; Wang, B.; Sui, M.L.; Yan, P.F. Cross-scale deciphering thermal failure process of Ni-rich layered cathode. *Nano Energy* **2024**, *126*, 109685. [CrossRef]
46. Röder, P.; Baba, N.; Wiemhöfer, H.D. A detailed thermal study of a Li[Ni_{0.33}Co_{0.33}Mn_{0.33}]O₂/LiMn₂O₄-based lithium ion cell by accelerating rate and differential scanning calorimetry. *J. Power Sources* **2014**, *248*, 978–987. [CrossRef]
47. Liu, J.; Huang, Z.; Sun, J.; Wang, Q. Heat generation and thermal runaway of lithium-ion battery induced by slight overcharging cycling. *J. Power Sources* **2022**, *526*, 231136. [CrossRef]
48. Zhang, H.; Wang, L.; He, X.M. Trends in a study on thermal runaway mechanism of lithium-ion battery with LiNi_xMn_yCo_{1-x-y}O₂ cathode materials. *Battery Energy* **2022**, *1*, 20210011. [CrossRef]
49. Belharouak, I.; Lu, W.; Vissers, D.; Amine, K. Safety characteristics of Li(Ni_{0.8}Co_{0.15}Al_{0.05})O₂ and Li(Ni_{1/3}Co_{1/3}Mn_{1/3})O₂. *Electrochim. Commun.* **2006**, *8*, 329–335. [CrossRef]
50. Monteiro, I.F.; Pinto, R.S.; Silva, M.M.; Fidalgo-Marijuan, A.; Costa, C.M.; Lanceros-Méndez, S.; Gonçalves, R. Lithium-ion battery high performance cathode electrode based on LiFePO₄ and thermal sensitive microspheres with thermal shutdown properties. *J. Power Sources* **2024**, *614*, 234956. [CrossRef]
51. Ping, P.; Wang, Q.S.; Huang, P.F.; Li, K.; Sun, J.H.; Kong, D.P.; Chen, C.H. Study of the fire behavior of high-energy lithium-ion batteries with full-scale burning test. *J. Power Sources* **2015**, *285*, 80–89. [CrossRef]
52. Wang, J.; Li, Y.; Liu, F.; Fang, Z.; Gu, N.; Chen, B.; Yang, N.; Jia, Y. A comparative study of overcharge thermal runaway force-electrical-thermal characteristics and safety assessment of lithium batteries with different cathode materials. *Appl. Therm. Eng.* **2024**, *256*, 124092. [CrossRef]
53. Faulkner, J.; Tatarchuk, B.J. The enthalpic reaction limits of Li-ion battery chemistries within various operating regimes and environments. *J. Power Sources* **2025**, *635*, 236329. [CrossRef]
54. Nie, B.; Dong, Y.; Chang, L. The evolution of thermal runaway parameters of lithium-ion batteries under different abuse conditions: A review. *J. Energy Storage* **2024**, *96*, 112624. [CrossRef]
55. Hu, E.Y.; Bak, S.M.; Senanayake, S.D.; Yang, X.Q.; Nam, K.W.; Zhang, L.L.; Shao, M.H. Thermal stability in the blended lithium manganese oxide—Lithium nickel cobalt manganese oxide cathode materials: An in situ time-resolved X-Ray diffraction and mass spectroscopy study. *J. Power Sources* **2015**, *277*, 193–197. [CrossRef]
56. Qi, C.B.; Wang, H.W.; Li, M.H.; Li, C.; Li, Y.L.; Shi, C.; Wei, N.N.; Wang, Y.; Zhang, H.P. Research on the Thermal Runaway Behavior and Flammability Limits of Sodium-Ion and Lithium-Ion Batteries. *Batteries* **2025**, *11*, 24. [CrossRef]
57. Yu, Y.; Wang, J.; Zhang, P.; Zhao, J. A detailed thermal study of usual LiNi_{0.5}Co_{0.2}Mn_{0.3}O₂, LiMn₂O₄ and LiFePO₄ cathode materials for lithium ion batteries. *J. Energy Storage* **2017**, *12*, 37–44. [CrossRef]
58. El Moutchou, S.; Aziam, H.; Mansori, M.; Saadoune, I. Thermal stability of Lithium-ion batteries: Case study of NMC811 and LFP cathode materials. *Mater. Today Proc.* **2022**, *51*, A1–A7. [CrossRef]
59. Zaghib, K.; Dubé, J.; Dallaire, A.; Galoustov, K.; Guerfi, A.; Ramanathan, M.; Benmaya, A.; Prakash, J.; Mauger, A.; Julien, C.M. Enhanced thermal safety and high power performance of carbon-coated LiFePO₄ olivine cathode for Li-ion batteries. *J. Power Sources* **2012**, *219*, 36–44. [CrossRef]
60. Park, J.-S.; Oh, S.-M.; Sun, Y.-K.; Myung, S.-T. Thermal properties of fully delithiated olivines. *J. Power Sources* **2014**, *256*, 479–484. [CrossRef]

61. Nam, K.W.; Bak, S.M.; Hu, E.Y.; Yu, X.Q.; Zhou, Y.N.; Wang, X.J.; Wu, L.J.; Zhu, Y.M.; Chung, K.Y.; Yang, X.Q. Combining In Situ Synchrotron X-Ray Diffraction and Absorption Techniques with Transmission Electron Microscopy to Study the Origin of Thermal Instability in Overcharged Cathode Materials for Lithium-Ion Batteries. *Adv. Funct. Mater.* **2013**, *23*, 1047–1063. [CrossRef]
62. Wu, Q.; Zhang, B.; Lu, Y. Progress and perspective of high-voltage lithium cobalt oxide in lithium-ion batteries. *J. Energy Chem.* **2022**, *74*, 283–308. [CrossRef]
63. Lin, C.; Li, J.Y.; Yin, Z.W.; Huang, W.Y.; Zhao, Q.H.; Weng, Q.S.; Liu, Q.; Sun, J.L.; Chen, G.H.; Pan, F. Structural Understanding for High-Voltage Stabilization of Lithium Cobalt Oxide. *Adv. Mater.* **2024**, *36*, 2307404. [CrossRef] [PubMed]
64. Mao, N.; Wang, Z.R.; Chung, Y.H.; Shu, C.M. Overcharge cycling effect on the thermal behavior, structure, and material of lithium-ion batteries. *Appl. Therm. Eng.* **2019**, *163*, 114147. [CrossRef]
65. Wu, C.J.; Wu, Y.; Feng, X.N.; Wang, H.B.; Zhang, F.K.; Chen, S.Q.; Li, B.; Deng, T.; Ouyang, M.G. Ultra-high temperature reaction mechanism of $\text{LiNi}_{0.8}\text{Co}_{0.1}\text{Mn}_{0.1}\text{O}_2$ electrode. *J. Energy Storage* **2022**, *52*, 104870. [CrossRef]
66. Sun, Y.; Ren, D.S.; Liu, G.J.; Mu, D.B.; Wang, L.; Wu, B.R.; Liu, J.H.; Wu, N.N.; He, X.M. Correlation between thermal stabilities of nickel-rich cathode materials and battery thermal runaway. *Int. J. Energy Res.* **2021**, *45*, 20867–20877. [CrossRef]
67. Liu, S.; Ma, T.; Wei, Z.; Bai, G.; Liu, H.; Xu, D.; Shan, Z.; Wang, F. Study about thermal runaway behavior of high specific energy density Li-ion batteries in a low state of charge. *J. Energy Chem.* **2021**, *52*, 20–27. [CrossRef]
68. Liu, S.; Xiong, L.; He, C. Long cycle life lithium ion battery with lithium nickel cobalt manganese oxide (NCM) cathode. *J. Power Sources* **2014**, *261*, 285–291. [CrossRef]
69. Golubkov, A.W.; Fuchs, D.; Wagner, J.; Wiltsche, H.; Stangl, C.; Fauler, G.; Voitic, G.; Thaler, A.; Hacker, V. Thermal-runaway experiments on consumer Li-ion batteries with metal-oxide and olivin-type cathodes. *RSC Adv.* **2014**, *4*, 3633–3642. [CrossRef]
70. Zhang, H.; Zhang, J. An overview of modification strategies to improve $\text{LiNi}_{0.8}\text{Co}_{0.1}\text{Mn}_{0.1}\text{O}_2$ (NCM811) cathode performance for automotive lithium-ion batteries. *eTransportation* **2021**, *7*, 100105. [CrossRef]
71. Wang, H.; Du, Z.; Rui, X.; Wang, S.; Jin, C.; He, L.; Zhang, F.; Wang, Q.; Feng, X. A comparative analysis on thermal runaway behavior of $\text{Li}(\text{Ni}_x\text{Co}_y\text{Mn}_z)\text{O}_2$ battery with different nickel contents at cell and module level. *J. Hazard. Mater.* **2020**, *393*, 122361. [CrossRef] [PubMed]
72. Shen, H.; Wang, H.; Li, M.; Li, C.; Zhang, Y.; Li, Y.; Yang, X.; Feng, X.; Ouyang, M. Thermal Runaway Characteristics and Gas Composition Analysis of Lithium-Ion Batteries with Different LFP and NCM Cathode Materials under Inert Atmosphere. *Electronics* **2023**, *12*, 1603. [CrossRef]
73. Zhao, L.; Hou, J.; Feng, X.; Xu, J.; Xu, C.; Wang, H.; Liu, H.; Hou, B.; Rui, X.; Gu, Y.; et al. The trade-off characteristic between battery thermal runaway and combustion. *Energy Storage Mater.* **2024**, *69*, 103380. [CrossRef]
74. Ahmed, S.; Nelson, P.A.; Gallagher, K.G.; Susarla, N.; Dees, D.W. Cost and energy demand of producing nickel manganese cobalt cathode material for lithium ion batteries. *J. Power Sources* **2017**, *342*, 733–740. [CrossRef]
75. Cui, Z.H.; Manthiram, A. Thermal Stability and Outgassing Behaviors of High-nickel Cathodes in Lithium-ion Batteries. *Angew. Chem.-Int. Ed.* **2023**, *62*, e202307243. [CrossRef]
76. Jo, M.; Park, S.H.; Lee, H. Effects of a Sodium Phosphate Electrolyte Additive on Elevated Temperature Performance of Spinel Lithium Manganese Oxide Cathodes. *Materials* **2021**, *14*, 4670. [CrossRef]
77. Bak, S.-M.; Hu, E.; Zhou, Y.; Yu, X.; Senanayake, S.D.; Cho, S.-J.; Kim, K.-B.; Chung, K.Y.; Yang, X.-Q.; Nam, K.-W. Structural Changes and Thermal Stability of Charged $\text{LiNi}_x\text{Mn}_y\text{Co}_z\text{O}_2$ Cathode Materials Studied by Combined In Situ Time-Resolved XRD and Mass Spectroscopy. *ACS Appl. Mater. Interfaces* **2014**, *6*, 22594–22601. [CrossRef]
78. Ohneseit, S.; Finster, P.; Floras, C.; Lubenau, N.; Uhlmann, N.; Seifert, H.J.; Ziebert, C. Thermal and Mechanical Safety Assessment of Type 2170 Lithium-Ion Batteries with NMC, NCA and LFP Cathodes—Investigation of Cell Abuse by Means of Accelerating Rate Calorimetry (ARC). *Batteries* **2023**, *9*, 237. [CrossRef]
79. Wang, S.; Song, L.; Li, C.; Tian, J.; Jin, K.; Duan, Q.; Wang, Q. Experimental study of gas production and flame behavior induced by the thermal runaway of 280 Ah lithium iron phosphate battery. *J. Energy Storage* **2023**, *74*, 109368. [CrossRef]
80. Xiao, Y.; Zhao, J.R.; Yin, L.; Li, B.; Tian, Y. Staged thermal runaway behaviours of three typical lithium-ion batteries for hazard prevention. *J. Therm. Anal. Calorim.* **2024**, *149*, 10321–10333. [CrossRef]
81. Jiang, J.; Dahn, J.R. ARC studies of the thermal stability of three different cathode materials: LiCoO_2 ; $\text{Li}[\text{Ni}_{0.1}\text{Co}_{0.8}\text{Mn}_{0.1}]\text{O}_2$; and LiFePO_4 , in LiPF_6 and LiBOB EC/DEC electrolytes. *Electrochim. Commun.* **2004**, *6*, 39–43. [CrossRef]
82. Zhang, F.; Wu, C.; Li, K.; Deng, T. A Comparative Analysis on Thermal Stability of Delithiated Nickel-Rich $\text{LiNi}_{0.8}\text{Co}_{0.15}\text{Al}_{0.05}\text{O}_2$ and $\text{LiNi}_{0.8}\text{Co}_{0.1}\text{Mn}_{0.1}\text{O}_2$ in Pouch Cells. *J. Electrochem. Energy Convers. Storage* **2023**, *21*, 011006. [CrossRef]
83. Zhang, Z.; Fouchard, D.; Rea, J.R. Differential scanning calorimetry material studies: Implications for the safety of lithium-ion cells. *J. Power Sources* **1998**, *70*, 16–20. [CrossRef]
84. Xiang, H.F.; Wang, H.; Chen, C.H.; Ge, X.W.; Guo, S.; Sun, J.H.; Hu, W.Q. Thermal stability of LiPF_6 -based electrolyte and effect of contact with various delithiated cathodes of Li-ion batteries. *J. Power Sources* **2009**, *191*, 575–581. [CrossRef]

85. Liang, C.; Zhang, W.H.; Wei, Z.S.; Wang, Z.Y.; Wang, Q.S.; Sun, J.H. Transition-metal redox evolution and its effect on thermal stability of $\text{LiNi}_x\text{Co}_y\text{Mn}_z\text{O}_2$ based on synchrotron soft X-ray absorption spectroscopy. *J. Energy Chem.* **2021**, *59*, 446–454. [[CrossRef](#)]
86. Peng, P.; Jiang, F. Thermal safety of lithium-ion batteries with various cathode materials: A numerical study. *Int. J. Heat Mass Transf.* **2016**, *103*, 1008–1016. [[CrossRef](#)]
87. GB 38031-2025; Safety Requirements for Traction Batteries of Electric Vehicles. Standardization Administration of the People's Republic of China: Beijing, China, 2025.
88. Wei, D.; Zhang, M.; Zhu, L.; Chen, H.; Huang, W.; Yao, J.; Yuan, Z.; Xu, C.; Feng, X. Study on Thermal Runaway Behavior of Li-Ion Batteries Using Different Abuse Methods. *Batteries* **2022**, *8*, 201. [[CrossRef](#)]
89. An, Z.; Li, W.; Du, X.; Jia, L.; Li, Q.; Zhang, D. Experimental study on behaviors of lithium-ion cells experiencing internal short circuit and thermal runaway under nail penetration abuse condition. *Appl. Therm. Eng.* **2024**, *247*, 123058. [[CrossRef](#)]
90. Liu, J.; Zhang, Y.; Zhou, L.; Han, C.; He, T.; Wang, Z. Influencing factors of lithium-ion battery thermal runaway in confined space. *J. Energy Storage* **2023**, *73*, 109125. [[CrossRef](#)]
91. Mao, N.; Gadkari, S.; Wang, Z.R.; Zhang, T.; Bai, J.L.; Cai, Q. A comparative analysis of lithium-ion batteries with different cathodes under overheating and nail penetration conditions. *Energy* **2023**, *278*, 128027. [[CrossRef](#)]
92. Wang, J.; Wang, C.; Sun, R.; Han, C.; Li, K.; Zhang, L.; Zhang, Y.; Guo, D.; Li, S.; Wang, Z.; et al. Thermal runaway and jet flame features of 314 Ah lithium iron phosphate battery: Mechanism exploration and safety assessment. *Appl. Therm. Eng.* **2025**, *272*, 126371. [[CrossRef](#)]
93. Jeon, M.; Lee, E.; Park, H.; Yoon, H.; Keel, S. Effect of Thermal Abuse Conditions on Thermal Runaway of NCA 18650 Cylindrical Lithium-Ion Battery. *Batteries* **2022**, *8*, 196. [[CrossRef](#)]
94. Chai, Z.X.; Li, J.Q.; Liu, Z.M.; Liu, Z.N.; Jin, X. Experimental analysis and safety assessment of thermal runaway behavior in lithium iron phosphate batteries under mechanical abuse. *Sci. Rep.* **2024**, *14*, 8673. [[CrossRef](#)] [[PubMed](#)]
95. Zhao, C.P.; Sun, J.H.; Wang, Q.S. Thermal runaway hazards investigation on 18650 lithium-ion battery using extended volume accelerating rate calorimeter. *J. Energy Storage* **2020**, *28*, 101232. [[CrossRef](#)]
96. Wang, G.Q.; Ping, P.; Kong, D.P.; Peng, R.Q.; He, X.; Zhang, Y.; Dai, X.Y.; Wen, J. Advances and challenges in thermal runaway modeling of lithium-ion batteries. *Innovation* **2024**, *5*, 100624. [[CrossRef](#)] [[PubMed](#)]
97. Mallick, S.; Gayen, D. Thermal behaviour and thermal runaway propagation in lithium-ion battery systems—A critical review. *J. Energy Storage* **2023**, *62*, 106894. [[CrossRef](#)]
98. Wang, H.B.; Liu, B.; Xu, C.S.; Jin, C.Y.; Li, K.J.; Du, Z.M.; Wang, Q.Z.; Ouyang, M.G.; Feng, X.N. Dynamic thermophysical modeling of thermal runaway propagation and parametric sensitivity analysis for large format lithium-ion battery modules. *J. Power Sources* **2022**, *520*, 230724. [[CrossRef](#)]
99. Li, Y.T.; Wang, H.B.; Wang, S.L.; Xu, L.J.; Li, Y.; Sun, J.L.; Gao, Y. Thermal Runaway Propagation Characteristics of Lithium-Ion Batteries with Different Cathode Materials: A Comparative Study. *Fire Technol.* **2025**, *61*, 1–22. [[CrossRef](#)]
100. Wang, H.B.; Xu, H.; Zhang, Z.L.; Wang, Q.Z.; Jin, C.Y.; Wu, C.J.; Xu, C.S.; Hao, J.Y.; Sun, L.; Du, Z.M.; et al. Fire and explosion characteristics of vent gas from lithium-ion batteries after thermal runaway: A comparative study. *Transportation* **2022**, *13*, 100190. [[CrossRef](#)]

Disclaimer/Publisher's Note: The statements, opinions and data contained in all publications are solely those of the individual author(s) and contributor(s) and not of MDPI and/or the editor(s). MDPI and/or the editor(s) disclaim responsibility for any injury to people or property resulting from any ideas, methods, instructions or products referred to in the content.